# A Model of a Tidally Synchronized Solar Dynamo

F. Stefani[1] · A. Giesecke[1] · T. Weier[1]

**Abstract** We discuss a solar dynamo model of Tayler–Spruit type whose $\Omega$-effect is conventionally produced by a solar-like differential rotation but whose $\alpha$-effect is assumed to be periodically modulated by planetary tidal forcing. This resonance-like effect has its rationale in the tendency of the current-driven Tayler instability to undergo intrinsic helicity oscillations which, in turn, can be synchronized by periodic tidal perturbations. Specifically, we focus on the 11.07-years alignment periodicity of the tidally dominant planets Venus, Earth, and Jupiter, whose persistent synchronization with the solar dynamo is briefly touched upon. The typically emerging dynamo modes are dipolar fields, oscillating with a 22.14-years period or pulsating with a 11.07-years period, but also quadrupolar fields with corresponding periodicities. In the absence of any constant part of $\alpha$, we prove the sub-critical nature of this Tayler–Spruit type dynamo. The resulting amplitude of the $\alpha$ oscillation that is required for dynamo action turns out to lie in the order of $1\,\mathrm{m\,s^{-1}}$, which seems not implausible for the Sun. When starting with a more classical, non-periodic part of $\alpha$, even less of the oscillatory $\alpha$ part is needed to synchronize the entire dynamo. Typically, the dipole solutions show butterfly diagrams, although their shapes are not convincing yet. Phase coherent transitions between dipoles and quadrupoles, which are reminiscent of the observed behavior during the Maunder minimum, can easily be triggered by long-term variations of dynamo parameters, but may also occur spontaneously even for fixed parameters. Further interesting features of the model are the typical second intensity peak and the intermittent appearance of reversed helicities in both hemispheres.

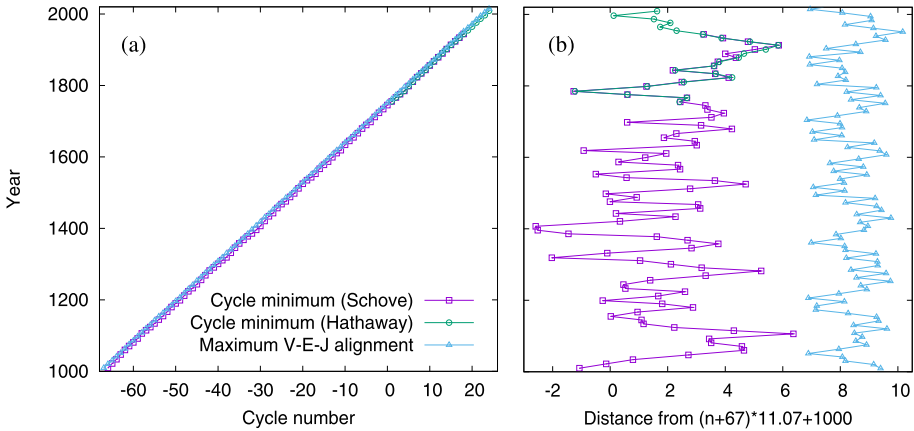**Keywords** Solar cycle · Models helicity · Theory

## 1. Introduction

Asking "Is there a chronometer hidden deep in the Sun?", Dicke (1978) had analyzed the similarity of the solar cycle with either a random walk process or, alternatively, a clocked

✉ F. Stefani
F.Stefani@hzdr.de

[1] Helmholtz-Zentrum Dresden-Rossendorf, Bautzner Landstr. 400, 01328 Dresden, Germany

**Figure 1** (**a**) Time series of the minima of the solar cycle according to Schove (1955, 1983) and Hathaway (2010), and of the maximum alignment of the Venus–Earth–Jupiter system. (**b**) Deviation of the time series from a linear function $f(n) = 11.07(n + 67) + 1000$ of the cycle number $n$.

process being perturbed by random fluctuations. While his statistical results pointed in favor of a clocked process, with shorter cycles usually being followed by longer ones as if the Sun remembered the correct phase, his conclusion was later criticized by Gough (1990) and Hoyng (1996) as relying on a too short time series of just 25 cycles.

The closely related discussion, initiated by Wolf (1859) and later entered by Bollinger (1952), Takahashi (1968), Wood (1972), Öpik (1972), Condon and Schmidt (1975), Grandpierre (1996), Palus *et al.* (2000), Hung (2007), Wilson (2013), Okhlopkov (2014), Poluianov and Usoskin (2014), of whether the Hale cycle of the Sun is synchronized with the 11.07-years alignment cycle of the tidally dominant planets Venus, Earth and Jupiter, was recently fueled by Okhlopkov (2016) who demonstrated an amazing parallelism of both time series for the last 1000 years.

In Figure 1(a) we illustrate the sequence $t_n$ of the solar minima, as taken from Schove (1955, 1983) and Hathaway (2010), together with the corresponding sequence of the maximum Venus–Earth–Jupiter alignments according to Okhlopkov (2016), which we have re-calculated and confirmed for the last 1000 years. In Figure 1(b) we show in detail the deviations (or residuals) $\delta_n = t_n - ((n + 67) \times 11.07 + 1000)$ of the three time series from a linear function of the cycle number $n$, with a presumed cycle duration of 11.07 years. Note the persistent closeness of the solar cycle to this linear curve, which does not even change during the Maunder (Beer, Tobias, and Weiss, 1998) and Spörer (Miyahara *et al.*, 2006) minima. While there is no evidence for any *local clocking* between the maximum Venus–Earth–Jupiter alignments and the cycle duration, both data sets remain *globally clocked*, with the solar minima instants never leaving a $\pm 4.5$-years band around the linear trend with 11.07-years period.

If we take those data of Schove and Hathaway (with all due caveats regarding their reliableness and accuracy before the year 1600, say), we can recompute Dicke's ratio $\sum_{i=n}^{24} \delta_i^2 / \sum_{i=n}^{24} (\delta_i - \delta_{i-1})^2$ of the mean square of the residuals $\delta_i$ to the mean square of the differences $\delta_i - \delta_{i-1}$ between two subsequent residuals. As stated by Dicke, the dependence of this ratio on the number $N = 24 - n + 1$ of cycles taken into account reads $(N + 1)(N^2 - 1)/(3(5N^2 + 6N - 3))$ for a random walk process and $(N^2 - 1)/(2(N^2 + 2N + 3))$ for a clocked process. Hence, for $N \to \infty$, the random walk ratio converges towards $N/15$, while
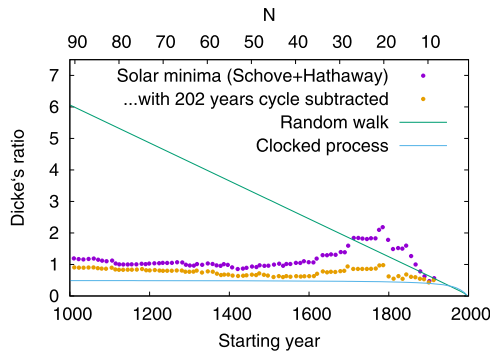
**Figure 2** Dicke's ratio between the mean square of the residuals to the mean square of the differences of two subsequent residuals in dependence on the number $N$ of cycles taken into account, for a random walk process (*green line*, converging towards $N/15$), a clocked process (*blue line*, converging towards 0.5), and the real solar cycle minima data (*violet dots*) from Schove and Hathaway. Despite the deterioration of the data's reliableness and accuracy for the time before 1600, a tendency towards a clocked process can still be observed. This becomes even more pronounced (*orange dots*) when a data-fitted Suess–de Vries type cycle (yielding a period of 202 years) is subtracted from the data.

the clocked process ratio converges to 0.5. Both curves are shown in Figure 2, together with Dicke's ratio computed for the actual Schove/Hathaway data (violet dots). While Dicke's original database was restricted to 25 cycles starting approximately at 1705, which made it hard to draw a solid conclusion about the character of the process, the enlarged database of Schove indicates that the real process proceeds (for large $N$) much closer to a clocked process than to a random walk process.

This feature becomes even more pronounced (orange dots) if we first subtract from the data a noticeable Suess–de Vries type cycle (yielding a period of 202 years when fitted to the Schove/Hathaway data between the years 1000 and 2009). Then the overshoot peak around the year 1800 is strongly reduced. Down to the year 1400 a further convergence towards the ultimate value 0.5 could even be expected, and the slight increase prior to this year might be guessed to be caused by the deteriorating accuracy of a data. At any rate, it seems worthwhile (but goes far beyond the scope of this paper) to look for better quality data for those early years, and to study the influence of the long-term cycles (Gleissberg, Suess–de Vries, Eddy) in a more systematic manner.

However impressive that coincidence of the solar cycle with a clocked process in general, and with the maximum Venus–Earth–Jupiter alignments in particular, may look like: the counter-arguments against any sort of external synchronization are serious as well. Indeed, the typical tidal acceleration of those planets (in the order of $10^{-10}$ m s$^{-2}$) is tiny compared to other acceleration terms in the Sun (Condon and Schmidt, 1975; De Jager and Versteegh, 2005; Callebaut, de Jager, and Duhau, 2012). Even if the typical tidal height of $h_{\text{tidal}} = Gm R_{\text{tacho}}^2 / (g_{\text{tacho}} d^3) \approx 1$ mm (exerted by a planet of mass $m$ at distance $d$ from the Sun) could be fully translated into a corresponding velocity of $v \sim (2 g_{\text{tacho}} h_{\text{tidal}})^{1/2} \approx 1$ m s$^{-1}$ (employing the huge gravity at the tachocline of $g_{\text{tacho}} \approx 500$ m s$^{-2}$ Wood, 2010), a physically realistic synchronization mechanism based on these tides is still hardly conceivable.

Although the competing forces in the convection zone are prohibitively large for any planetary synchronization mechanism to get a chance to work there, things may be more subtle in the stably stratified tachocline region. A promising idea about a putative planetary influence, as first discussed by Abreu *et al.* (2012), relies on periodic tidal perturbations of the adiabaticity in the tachocline region, whose value is decisive for its storage capacity for

magnetic flux tubes. While primarily discussed with view on long-term modulations of the solar dynamo, there is no prior reason not to apply the same concept to the basic Hale cycle as well. In a recent paper (Stefani *et al.*, 2018) we made a first attempt to validate this idea in the framework of a simplified Babcock–Leighton type model, employing the time-delay concept of Wilmot-Smith *et al.* (2006). Specifically, the tidal perturbations were emulated as periodic changes of the critical magnetic field strength beyond which flux tubes would erupt to the solar surface. Although our results, obtained in a limited parameter region, were essentially negative, we still consider this synchronization mechanism as rather attractive, and would like to encourage further work in this direction.

Yet another promising synchronization mechanism was first delineated by Weber *et al.* (2015) and later corroborated in detail by Stefani *et al.* (2016, 2018). It starts from the numerical observation that the current-driven, kink-type Tayler instability (TI) (Tayler, 1973; Pitts and Tayler, 1985; Gellert, Rüdiger, and Hollerbach, 2011; Seilmayer *et al.*, 2012; Rüdiger, Kitchatinov, and Hollerbach, 2013; Rüdiger *et al.*, 2015b; Stefani and Kirillov, 2015) has an intrinsic tendency for oscillations of the helicity and the $\alpha$-effect related to it.

At this point, a few general remarks on kink-type instabilities, and their applicability to stellar dynamo models, may be appropriate: the notion Tayler–Spruit dynamo referred originally to the idea of Spruit (2002) who had proposed a non-linear, sub-critical dynamo in which the poloidal-to-toroidal field transformation is conventionally accomplished by the $\Omega$-effect, while the toroidal-to-poloidal transformation starts only when the toroidal field acquires sufficient strength to become unstable to the non-axisymmetric, current-driven TI. A fundamental flaw of this dynamo concept was revealed by Zahn, Brun, and Mathis (2007) who argued that any emerging non-axisymmetric ($m = 1$) TI mode would be topologically unsuitable for regenerating the dominant axisymmetric ($m = 0$) toroidal field. Fortunately, the same authors offered a possible remedy for the Tayler–Spruit dynamo concept provided that the $m = 1$ TI would produce an $\alpha$-effect (comprising some $m = 0$ component). In hindsight, it appears that this idea had been investigated more than a decade earlier by Ferriz Mas, Schmitt, and Schüssler (1994). Working in the flux-tube approximation, these authors had derived the $\alpha$-effect connected with the kink-instability and pointed out its crucial importance for closing the dynamo loop.

Beyond the flux-tube approximation, the existence of any TI-related $\alpha$-effect is still a matter of debate. Various authors (Chatterjee *et al.*, 2011; Gellert, Rüdiger, and Hollerbach, 2011; Bonanno *et al.*, 2012; Bonanno and Guarnieri, 2017) had evidenced spontaneous symmetry breaking between left- and right-handed TI modes, leading indeed to a finite value of $\alpha$, but mainly for comparably large values of the magnetic Prandtl number [$Pm$], *i.e.*, the ratio between viscosity and magnetic diffusivity. Things are different, though, for the case of low $Pm$, as it is typical for the solar tachocline region where $Pm$ is believed to lie in the range $10^{-3} - 10^{-2}$. In this limit of small $Pm$, we had numerically observed (although in the simplified geometry of a full cylinder) a tendency of the TI to undergo *oscillations* of the helicity and the $\alpha$-effect (Weber *et al.*, 2013, 2015). Remarkably, those oscillations between left- and right-handed $m = 1$ TI modes do barely change the energy content of the instability, which makes them very susceptible to weak $m = 2$ perturbations (Stefani *et al.*, 2016). This fact may indeed be the key for the easy synchronizability of the $\alpha$-effect with the tiny tidal forces as exerted by planets.

The resonant reaction of $\alpha$ on tidal excitations was later incorporated into a very simple ordinary differential equation (ODE) model of an $\alpha$–$\Omega$ dynamo which turned out to produce oscillations with period doubling (Stefani *et al.*, 2016). In this way it was argued that the 11.07-years tidal perturbations could lead to a resonant excitation of a 11.07-years oscillation of the TI-related $\alpha$-effect, and thereby to a 22.14-years Hale cycle of the entire dynamo.

In Stefani *et al.* (2018), it was specified that such field *oscillations* occur only in certain bands of the magnetic diffusion time $\tau$, while for intervening bands they were replaced by field *pulsations* with 11.07-years period. Noteworthy was the persistent phase coherence when passing from oscillations to pulsations, and back. What could not be resolved by this simple ODE system (despite some progress in Stefani *et al.*, 2017) was the spatio-temporal specifics of the transitions between oscillations and pulsations, for which higher-dimensional modeling is definitely required.

As a sequel to Stefani *et al.* (2016, 2018), the present paper investigates this spatio-temporal behavior of a tidally synchronized dynamo of the Tayler–Spruit type. For that purpose, we replace the ODE system by a partial differential equation (PDE) system with the co-latitude as the only spatial variable. Similar radially averaged, pseudo-Cartesian models (although without any synchronization aspect) have been studied by many authors (Parker, 1955; Schmalz and Stix, 1991; Jennings and Weiss, 1991; Roald and Thomas, 1997; Kuzanyan and Sokoloff, 1997), which will allow us, in Section 2 and the Appendix, to compare and validate our numerical method.

In Section 3, we will analyze in detail a synchronized, sub-critical dynamo of Tayler–Spruit type in its purest form. For that purpose, we use a latitudinal dependence of the $\Omega$-effect as inferred from helioseismology (Charbonneau *et al.*, 1999), and restrict the $\alpha$-effect to its 11.07-years periodic part whose amplitude has the same resonance-like dependence on the toroidal field as originally proposed in Stefani *et al.* (2016). Since, for weak fields, this resonance term is proportional to the square of the field, it cannot yield a linear instability. Instead, the dynamo needs some finite field amplitude to start off. Apart from a detailed discussion of the dependence of this sub-critical dynamo on the initial conditions, we will also argue that the typical resulting amplitudes of $\alpha$ are on the order of $1 \, \text{m s}^{-1}$, which seems not unrealistic for the solar dynamo. Depending on some parameter choices, the arising fields are dipoles or quadrupoles, which can either oscillate with a 22.14-years period or pulsate with an 11.07-years period. We also observe intermediate states between oscillations and pulsations, which are reminiscent of the Gnevyshev–Ohl rule (Gnevyshev and Ohl, 1948), which states that the sunspot numbers over an odd cycle exceeds that of the preceding even cycle. During transitions between dipoles and quadrupoles, hemispherical dynamos are partly observed, too.

The oscillatory dipole solutions show, for high latitudes, poleward migration ("rush to the poles"), and for low latitudes a sort of butterfly diagram in the correct direction, although its form is not completely convincing yet. Further interesting features to be discussed here are a second intensity maximum, comparable to the double peak of the solar dynamo, and the intermediate appearance of reversed helicities in the two hemispheres. The latter fact, which is a direct consequence of the synchronized, oscillatory character of $\alpha$, might be related to the current-helicity observations of Zhang *et al.* (2010), Pipin *et al.* (2013).

In Section 4, we will soften the pure Tayler–Spruit principle by combining the periodic part of $\alpha$ with a more standard, non-periodic term that is asymmetric with respect to the equator and only quenched by the toroidal field in the conventional manner. In the limiting case of a conventional $\alpha$–$\Omega$ dynamo we obtain dipoles or quadrupoles with typical periods between 20 and 40 years. When adding to this standard dynamo our resonant periodic $\alpha$ term, we can easily enslave the dynamo to the 22.14-years periodicity, partly with some intermediate 2:3 synchronization to a 33.21-years period. Remarkably, the amplitude of the oscillatory part of $\alpha$ that is required for this synchronization turns out to be significantly smaller (below $1 \, \text{m s}^{-1}$) than the typical values needed for the purely non-linear dynamo as discussed above. By increasing the oscillatory part of $\alpha$ we obtain then a sequence of oscillatory quadrupoles, hemispherical dynamos, dipoles with a strong Gnevyshev–Ohl tendency,

and regularly oscillating dipoles. When adding some noise to the non-periodic $\alpha$ term, the conventional $\alpha$–$\Omega$ model and the synchronized "hybrid" model exhibit typical features of a random walk process and a clocked process, respectively, as will be illustrated by Dicke's ratio.

In Section 5, we show how long-term changes of various dynamo parameters (*e.g.*, the portion of the periodic $\alpha$ part or the term which governs field losses by magnetic buoyancy) are capable of producing transitions between dipole and quadrupole fields, a behavior for which some observational evidence exists from the Maunder minimum (Sokoloff and Nesme-Ribes, 1994; Arlt, 2009; Moss and Sokoloff, 2017; Weiss and Tobias, 2016). A robust feature of our synchronization model is the phase coherence which is maintained throughout such transitions.

The paper closes with a summary, a discussion of open questions, including the applicability of the general idea to other $m = 1$ instabilities or flow structures, in particular the recently discussed magneto-Rossby waves of the tachocline (McIntosh *et al.*, 2017; Dikpati *et al.*, 2017; Zaqarashvili, 2018), and a call for higher-dimensional simulations of this type of tidally synchronized solar dynamo model.

## 2. The Numerical Model

In this section we set-up the dynamo model and discuss its numerical implementation. We work with a system of partial differential equations, whose spatial variable is restricted to the solar co-latitude $\theta$. While similar models have been utilized by a number of authors (Parker, 1955; Schmalz and Stix, 1991; Jennings and Weiss, 1991; Roald and Thomas, 1997; Kuzanyan and Sokoloff, 1997), we use the specific formulation of Jennings and Weiss (1991).

We focus on the axisymmetric magnetic field which is split into a poloidal component $\mathbf{B}_P = \nabla \times (A\mathbf{e}_\phi)$ and a toroidal component $\mathbf{B}_T = B\mathbf{e}_\phi$. Introducing the helical turbulence parameter $\alpha$ and the radial derivative $\omega = \sin(\theta)\, \mathrm{d}(\Omega r)/\mathrm{d}r$ of the azimuthal velocity, we arrive at the one-dimensional $\alpha$–$\Omega$ dynamo model

$$\frac{\partial B(\theta,t)}{\partial t} = \omega(\theta,t)\frac{\partial A(\theta,t)}{\partial \theta} + \frac{\partial^2 B(\theta,t)}{\partial \theta^2} - \kappa B^3(\theta,t), \tag{1}$$

$$\frac{\partial A(\theta,t)}{\partial t} = \alpha(\theta,t)B(\theta,t) + \frac{\partial^2 A(\theta,t)}{\partial \theta^2}, \tag{2}$$

wherein $A(\theta,t)$ represents the vector potential of the poloidal field at co-latitude $\theta$ (running between 0 and $\pi$) and time $t$, and $B(\theta,t)$ the corresponding toroidal field. Here, $\alpha$ and $\omega$ denote the non-dimensionalized versions of the dimensional quantities $\alpha_{\mathrm{dim}}$ and $\omega_{\mathrm{dim}}$, according to $\alpha = \alpha_{\mathrm{dim}}R/\eta$ and $\omega = \omega_{\mathrm{dim}}R^2/\eta$, where $R$ is the radius of the considered dynamo region (we will later use here the radius of the tachocline) and $\eta$ is the magnetic diffusivity which is connected with the conductivity $\sigma$ via $\eta = 1/(\mu_o\sigma)$. The time is non-dimensionalized by the diffusion time, *i.e.*, $t = t_{\mathrm{dim}}\eta/R^2$.

The not so familiar term $\kappa B^3(\theta,t)$, as introduced by Jones (1983), Jennings and Weiss (1991), has been included to account for losses owing to magnetic buoyancy, on the assumption that the escape velocity is proportional to $B^2$. While this term is not essential for our synchronization model, it may provide a link to the idea of Abreu *et al.* (2012) that variations of the adiabaticity, and hence of the field storage capacity, in the tachocline could explain the effect of weak tidal forces on *long-term* variations of the solar dynamo.

The boundary conditions at the north and south pole are $A(0, t) = A(\pi, t) = B(0, t) = B(\pi, t) = 0$.

This PDE system is solved by a finite-difference scheme using the Adams–Bashforth method. We have validated the numerical method by checking the convergence and comparing it with some results of Jennings and Weiss (1991) for the paradigmatic case with $\alpha(\theta) = \alpha_0 \cos(\theta)$ and $\omega(\theta) = \omega_0 \sin(\theta)$. Even with such a simple model one can obtain butterfly diagrams, although one has to be careful with their interpretation. Details can be found in the Appendix.

Throughout the rest of the paper, we employ a $\theta$-dependence of the $\omega$-effect in the form

$$\omega(\theta) = \omega_0 \big(1 - 0.939 - 0.136 \cos^2(\theta) - 0.1457 \cos^4(\theta)\big) \sin(\theta), \tag{3}$$

as derived from helioseismological measurements (Charbonneau *et al.*, 1999; Charbonneau, 2010). Note that $\omega(\theta)$, which is changing sign at $\theta = 55°$ and $125°$, is assumed to be constant in time. We use a plausible value of $\omega_0 = 10\,000$ which results from taking the measured 460 nHz frequency at the equator, an estimated tachocline thickness of $1/10$ of its approximate radius $R = 5 \times 10^8$ m, and an assumed value of $\eta = 7.16 \times 10^7$ m$^2$ s$^{-1}$. This somewhat peculiar value, which lies close to the upper margin of the commonly used values $10^6 - 10^8$ m$^2$ s$^{-1}$ (Charbonneau, 2010) corresponds to a diffusion time $\tau = R^2/\eta = 110.7$ years, which is just a factor 10 times larger than the period of the tidal forcing.

Much less than for $\omega(\theta)$ is known for the corresponding distribution of the $\alpha$ effect which we, in general, suppose to comprise a non-periodic part $\alpha^c$ and a time-periodic part $\alpha^p$. The non-periodic contribution $\alpha^c$ represents the traditional $\alpha$ effect, which is related to the non-mirror symmetric part of the turbulence. It will be equipped with the typical north–south asymmetry and a simple algebraic quenching with the magnetic field strength, as it has been utilized in many solar dynamo models. The oscillatory contribution $\alpha^p$, however, relies on the observation (Weber *et al.*, 2015) that the TI at low magnetic Prandtl numbers (which applies to the tachocline) has a tendency to undergo oscillations of the helicity, and that those helicity oscillations can be resonantly excited by $m = 2$ tidal-like perturbations (Stefani *et al.*, 2016), without (or barely) changing the energy content of the instability. The specific forms of both parts of $\alpha$ will be discussed further below. At any rate, the saturation of the dynamo is exclusively accomplished by the magnetic field dependence, *i.e.*, the quenching of $\alpha$, while $\omega$ remains unchanged, as stated above.

## 3. Synchronizing a Pure Tayler–Spruit Dynamo Model

In this section, we illustrate the variety of dynamo solutions that arise under the influence of an $\alpha$-effect that is supposed to oscillate with a 11.07-years period and to have a specific $B$-dependent amplitude which reflects the resonance condition of the periodic tidal trigger with the intrinsic oscillation of the TI-related $\alpha$ effect (Weber *et al.*, 2015; Stefani *et al.*, 2016). By virtue of this $B$-dependence of $\alpha$, this model can only yield sub-critical dynamo action, a fact that will be proven in the following. The specific effects of combining the periodic $\alpha$-term with a more conventional, non-periodic $\alpha$-term will be assessed in the next section.

### 3.1. Specifying the $\alpha$-Effect

The time-periodic part $\alpha^p$ is actually at the root of our synchronization model. A serious uncertainty applies to the $\theta$-dependence of this term in general, and its equatorial symme-

try/asymmetry in particular. A closely related issue is its "smoothing" character, *i.e.*, whether and how $\alpha^p(\theta, t)$ depends also on $B$ at neighboring latitudes and previous times.

As a first attempt, we will use an $\alpha^p$-dependence on $B$ that is instantaneous in $t$ and local in $\theta$, the latter assumption corresponding to a sort of flux-tube approximation. In reality, some averaging over time and space, realized by integral kernels, seems more appropriate. Any concretization of this idea is, however, left for future work.

As for the latitudinal symmetry property of $\alpha^p$ we will start with the plausible assumption that it has the same north–south asymmetry as is usually assumed for the non-periodic part. This relies on the observation of Rüdiger, Kitchatinov, and Hollerbach (2013) that, under the additional influence of a poloidal field, the helicity of the TI-related $\alpha$-effect is governed by the pseudo-scalar $\mathbf{B} \cdot \nabla \times \mathbf{B}$ (rather than by the pseudo-scalar $\mathbf{g} \cdot \nabla \times \mathbf{\Omega}$, formed with the stratification vector $\mathbf{g}$ and the global rotation $\mathbf{\Omega}$). Although this argument applies, first of all, to the non-oscillatory part of $\alpha$ for which it predicts a positive value in the northern and a negative value in the southern hemisphere, we extend here this equatorial asymmetry also to the oscillatory part. That this is in no way self-evident, and should be scrutinized in future work, can be inferred from the work of Proctor (2007) who obtained for his fluctuating $\alpha-\Omega$ model an averaged induction term that is *symmetric* about the equator.

In contrast to Rüdiger, Kitchatinov, and Hollerbach (2013), we further assume that $\alpha^p$ is restricted to the $\pm 35°$ strip around the equator, since this is the region with positive radial shear where the TI may have time to develop, not being overrun by the faster magnetoro-tational instability (MRI) that might be dominant in the near-pole regions characterized by negative radial shear (Kagan and Wheeler, 2014; Jouve, Gastine, and Lignieres, 2015). While this restriction to the $\pm 35°$ strip sounds plausible also with view on the restriction of sunspots to this area, with regard to the key role of the $\pm 55°$ latitude region for starting the dynamo cycle (McIntosh, 2015), the entire argument might not be that convincing. We will come back to this point in the conclusions.

Thus motivated, we start with the following parametrization for $\alpha^p(\theta, t)$:

$$\alpha^p(\theta, t) = \alpha_0^p \sin(2\pi t/11.07) \frac{B^2(\theta, t)}{(1 + q_\alpha^p B^4(\theta, t))} S(\theta) \quad \text{for } 55° < \theta < 125°,$$

$$= 0 \quad \text{elsewhere}, \tag{4}$$

where the $B$-dependent term is supposed to have the typical resonance-type structure $\sim B^2/(1 + q_\alpha^p B^4)$ as already used in the ODE system (Stefani *et al.*, 2016). Note that the latitudinal dependence

$$S(\theta) = \text{sgn}(90° - \theta)$$

$$\times \left[ 1 - \left( 1 + \tanh\left(\frac{\theta/180° - 0.5}{0.2}\right)\right)\left(1 - \tanh\left(\frac{\theta/180° - 0.5}{0.2}\right)\right)\right] \tag{5}$$

comprises a smoothing term around the equator in order to avoid a numerically inconvenient steep jump of $\alpha$ here.

At any rate, $\alpha^p(\theta, t)$ is not pre-given but co-evolves with the solution of the PDE system. For its interpretation we recall the connection to the dimensional value, $\alpha = \alpha_{\text{dim}} R/\eta$, which leads (with $R = 5 \times 10^8$ m, $\eta = 7.16 \times 10^7$ m$^2$ s$^{-1}$) to $\alpha_{\text{dim}} = \alpha/6.98$ m s$^{-1}$. That is, all values shown in the following figures should be divided by a factor 7 to get the physical value $\alpha_{\text{dim}}$ in m s$^{-1}$. Note that, since we have used a comparably high value of $\eta$, the resulting values of $\alpha_{\text{dim}}$ should be considered an upper limit and might in reality be significantly smaller. The constant term $\alpha_0^c$ is set to a very small, but non-zero value of 0.001.
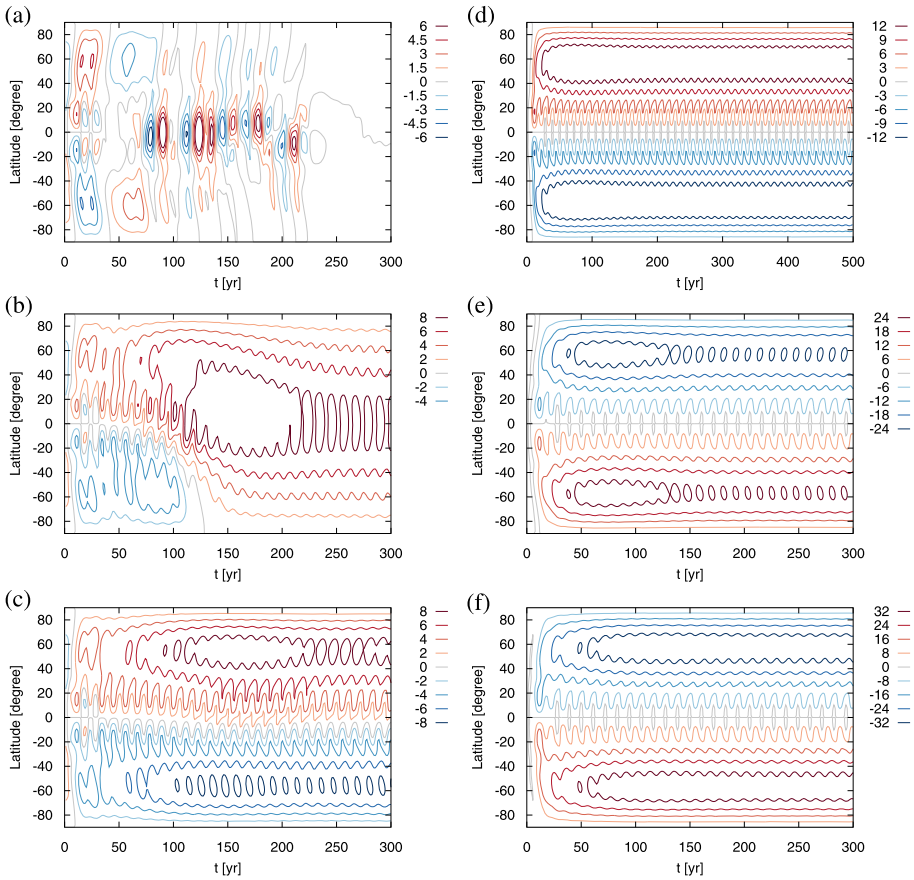
**Figure 3** Behavior of $B(\theta, t)$ of the synchronized Tayler–Spruit dynamo with a nearly pure periodic $\alpha^P$ term. The fixed parameters are $\omega_0 = 10\,000$, $\kappa = 0$, $\alpha_0^c = 0.001$ $q_\alpha^P = 0.2$, the initial conditions are $s = 3$ and $u = 0.001$, and the varying parameter is $\alpha_0^p = 16.1$ (**a**), 16.2 (**b**), 16.3 (**c**), 30 (**d**), 70 (**e**), 150 (**f**). Note that, here and throughout the paper, the ordinate axis represents not the co-latitude $\theta$ but the normal solar latitude $90° - \theta$.

Since for the sub-critical dynamo type to be studied here the initial conditions play an essential role, we state them explicitly:

$$A(\theta, 0) = s \sin(\theta) + u \sin(2\theta), \tag{6}$$

$$B(\theta, 0) = -s \sin(2\theta) - u \sin(\theta). \tag{7}$$

Both pre-factors $s$ and $u$, which denote symmetric and asymmetric components for $A$, are usually set to some non-zero value, in order not to suppress artificially any relevant modes.

### 3.2. The Case $\kappa = 0$

Figure 3 shows the behavior of $B(\theta, t)$ for the specific parameter choice $\omega_0 = 10\,000$, $\kappa = 0$, $q_\alpha^p = 0.2$, and the initial conditions $s = 3$ and $u = 0.001$, when varying the strength of the

**Figure 4** Behavior of $B(\theta, t)$ (**a**), $A(\theta, t)$ (**b**), and $\alpha(\theta, t)$ (**c**). Parameters as in Figure 3, but with $\alpha_0^p = 100$.
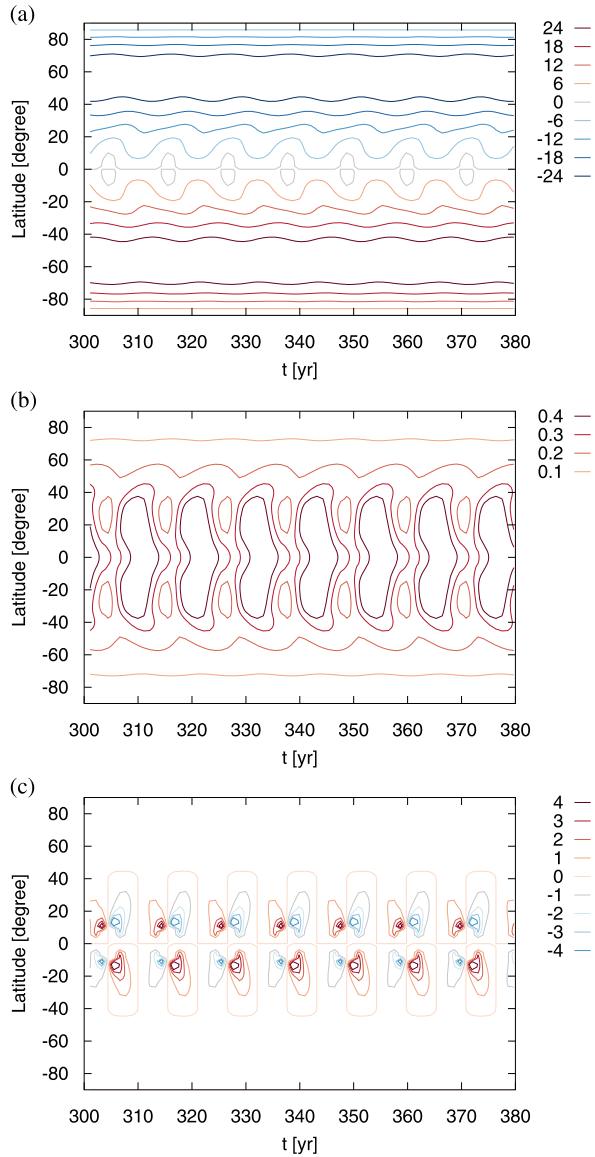


periodic $\alpha$ term, *i.e.*, $\alpha_0^p$ between 16.1 (a) and 150 (f). Evidently, the dynamo starts only for $\alpha_0^p = 16.2$ (b), while it still dies out for the slightly smaller value $\alpha_0^p = 16.1$ (a).

Also interesting is the distinction between a quadrupole, pulsating with 11.07-years period, which arises for $\alpha_0^p = 16.2$ (b), and the pulsating dipole (also with 11.07-years period) into which the field evolves for $\alpha_0^p = 16.3$ (c). This pulsating dipole persists then also for the three higher values $\alpha_0^p = 30$ (d), 70 (e), 150 (f).

Some detailed features of this dynamo behavior are illustrated in Figure 4 for another value $\alpha_0^p = 100$ (which would lie between panels (e) and (f) of Figure 3). Complementary to $B$ (a), the poloidal field $A$ (b) shows clearly the pulsating dipolar field structure. While $\omega$ is kept constant over time (see Equation 3), the behavior of $\alpha(\theta, t)$ (c) is more interesting:
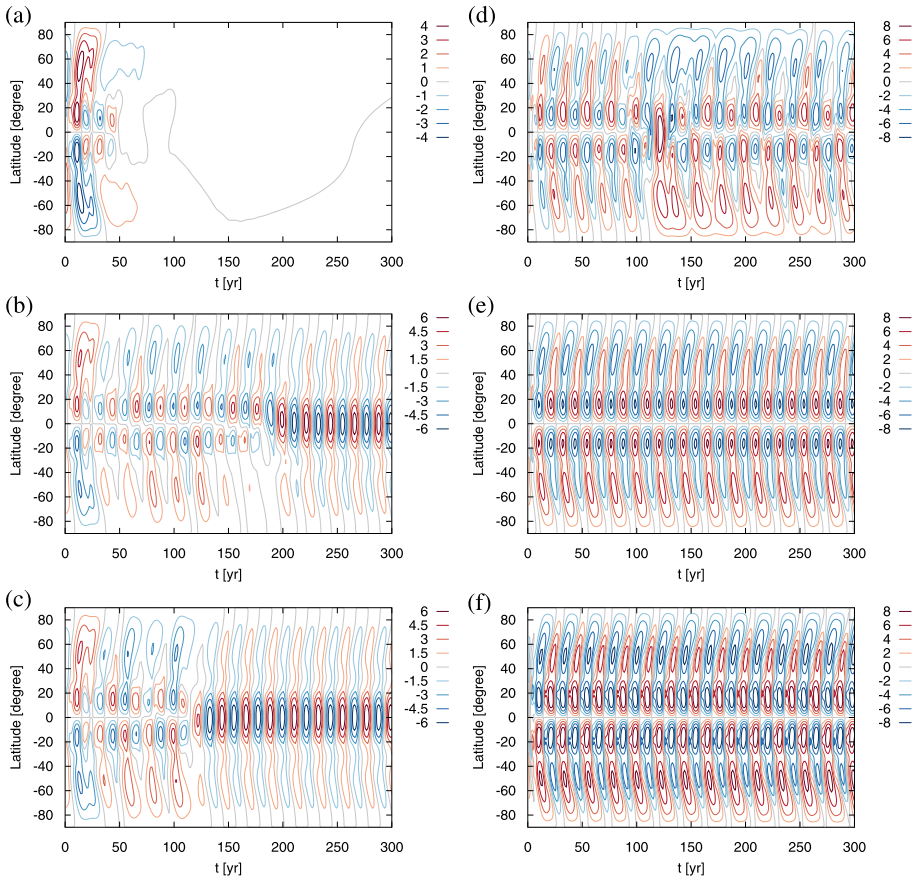
**Figure 5** Behavior of $B(\theta, t)$ of the synchronized Tayler–Spruit dynamo with a periodic $\alpha^p$ term. The fixed parameters are $\omega_0 = 10\,000$, $\kappa = 1$, $q_\alpha^p = 0.2$, the initial conditions are $s = 3$ and $u = 0.001$, and the varying parameter is $\alpha_0^p = 21.2$ (**a**), 21.5 (**b**), 23 (**c**), 50 (**d**), 70 (**e**), 150 (**f**).

Restricted, by construction, to the $\pm 35°$ strip around the equator (*i.e.*, $55° < \theta < 125°$), its dependence on $B$ leads to typical sign changes in both hemispheres, a feature that could possibly be linked to the reversed current helicity as intermittently observed on the Sun (Zhang *et al.*, 2010).

### 3.3. The Case $\kappa \neq 0$

Up to this point, the final state of the dynamo was, somewhat disappointing, either a pulsating quadrupole or a pulsating dipole. In the following we will also find oscillatory dipoles when going over to $\kappa \neq 0$, *i.e.*, when allowing for some magnetic field loss due to rising flux tubes. The results are illustrated for the specific choice $\kappa = 1$. With all remaining parameters unchanged (*i.e.*, $\omega_0 = 10\,000$, $q_\alpha^p = 0.2$, $s = 3$ and $u = 0.001$), Figure 5 shows the behavior of $B(\theta, t)$ when varying the amplitude of $\alpha_0^p$ now between 21.2 (a) and 150 (f). Evidently, since the additional field losses have to be compensated, the dynamo starts now only for $\alpha_0^p = 21.5$ (b), while dying out for the slightly smaller value $\alpha_0^p = 21.2$ (a).

**Figure 6** Behavior of
$B(\theta, t)$ (**a**), $A(\theta, t)$ (**b**), and
$\alpha(\theta, t)$ (**c**). Parameters as in
Figure 5, but with $\alpha_0^p = 100$.

(a)

(b)

(c)
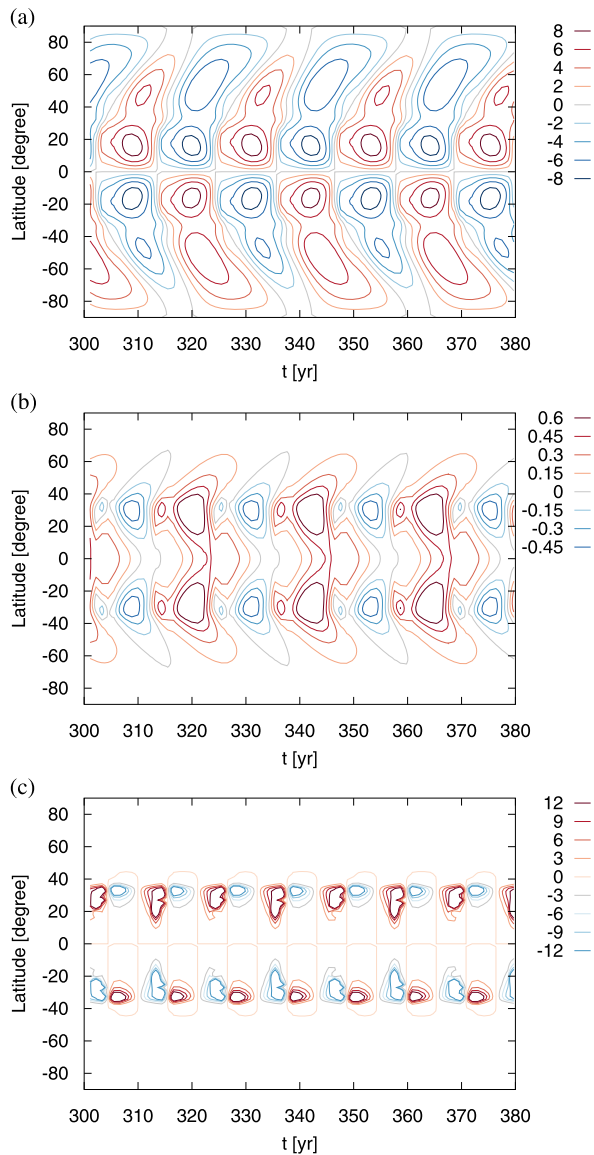


Whereas for $\alpha_0^p = 21.5$ (b) and $\alpha_0^p = 23$ (c) the initially prescribed dipole finally gives way to a quadrupole oscillating with 22.14-years period, for $\alpha_0^p = 50$ (d) it recovers after a short excursion (between $110 - 130$ years) to a hemispherical and quadrupolar mode. While such spontaneous dipole–quadrupole transitions are found here only in certain parameter regions, we will later see that they can easily be triggered by changing such parameters as the amplitude of $\alpha^p$ or the loss parameter $\kappa$. For $\alpha_0^p = 70$ (e) and $\alpha_0^p = 150$ (f) we obtain very regular dipole oscillations, although in either case with a clear Gnevyshev–Ohl tendency.

Again, we illustrate in Figure 6 the detailed behavior for the particular value $\alpha_0^p = 100$, which lies between panels (e) and (f) of Figure 5. Actually, the results exhibit some interesting features which are not untypical for the Sun. First, (a) shows for high latitudes the
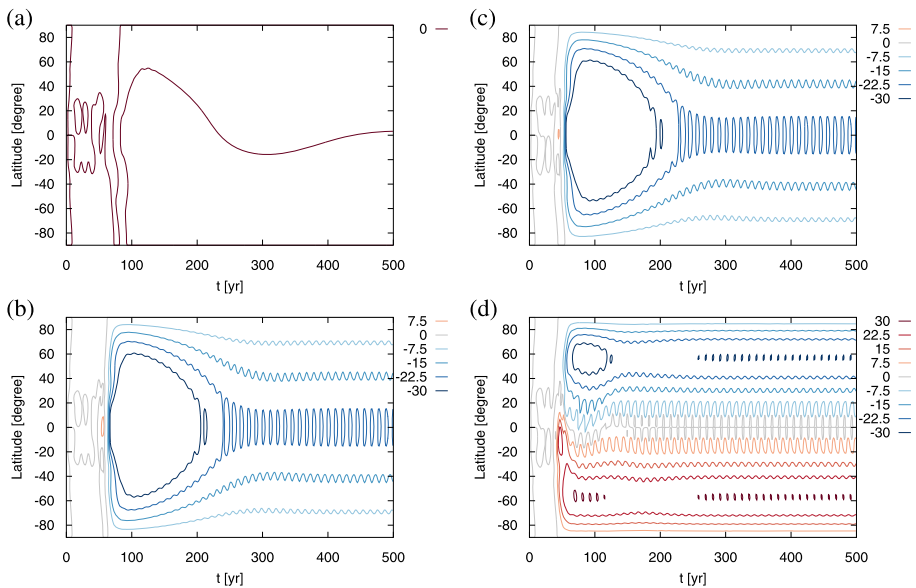
**Figure 7** Behavior of $B(\theta, t)$ of the synchronized $\alpha$–$\Omega$ model with the fixed values $\Omega_0 = 10\,000$, $\alpha_0^p = 100$, $\kappa = 0$, $q_\alpha^p = 0.2$, $u = 0.001$ and the variable initial conditions $s = 0.707$ (**a**), $0.708$ (**b**), $0.729$ (**c**) and $0.73$ (**d**).

typical "rush to the poles", while for low latitudes we see a sort of butterfly slightly tending equator-ward. Admittedly, the shape of this butterfly is not convincing yet, and it remains to be seen whether this shape can be improved in higher-dimensional simulations, including also the meridional circulation.

Second, the Gnevyshev–Ohl tendency becomes clearly visible with the "blue field" in the northern hemisphere being stronger than the "red field" (and *vice versa* in the southern hemisphere). Closely related to that feature, the $\alpha$ values in (c) show also some symmetry breaking between positive and negative values.

### 3.4. The Sub-critical Character of the Tayler–Spruit Dynamo

Now we address the sub-critical nature of the dynamo which is, in terms of a high sensitivity on the initial conditions, illustrated in Figure 7. We choose again $\omega_0 = 10\,000$, $\kappa = 0$, $q_\alpha^p = 0.2$, $u = 0.001$, but vary now the initial value of the dipole strength $s$ in a narrow interval between 0.707 and 0.73. The value of $\alpha_0^p = 100$ is chosen to lie between 70 (*cf.* Figure 3(e)) and 150 (Figure 3(f)). Remarkably, the dynamo starts only when $s \geq 0.708$ (b), while the slightly weaker initial perturbation $s = 0.707$ (a) dies away at large times. Further to this, between $s = 0.729$ (c) and $s = 0.73$ (d) the dynamo field changes from a pulsating quadrupole to a pulsating dipole.

The sub-critical behavior is summarized in Figure 8 which shows the dynamo threshold in the $\alpha_0^p$–$s$ plane, for the three specific loss parameters $\kappa = 0$, 0.5 and 1. Each of the points in this graphic has been determined by evaluating the dynamo/non-dynamo behavior at a few points in its vicinity. For large values of $\alpha_0^p$ we obtain the typical sub-critical $s \sim (\alpha_0^p)^{-0.5}$ behavior, which means that the necessary initial condition can be lowered (with the square-root) when the dynamo strength is increased. Also typical for a sub-critical bifurcation is the "rugged" left boundary, which is reminiscent of a similar fractal shape found for pipe flows

**Figure 8** Stability boundaries in the $\alpha_0^p - s$ plane, for the three values $\kappa = 0$, 0.5 and 1 and $q_\alpha^p = 0.2$, $u = 0.001$. Note the left "rugged" boundary at low values of $\alpha_0^p$. For large values of $\alpha_0^p$, the boundary converges to $s \sim (\alpha_0^p)^{-0.5}$.
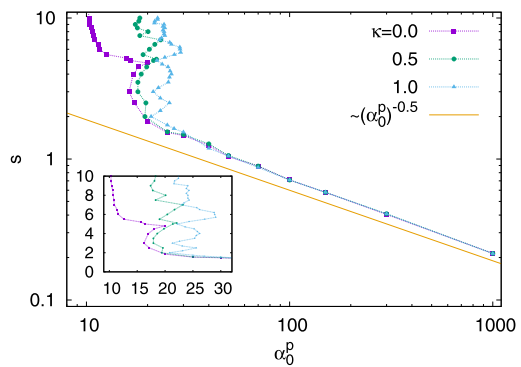


(Eckhardt *et al.*, 2008). We only mention here that a similar sub-critical behavior can also be obtained, with less numerical effort, for the ODE case.

## 4. Synchronizing a Hybrid Dynamo

Having verified the sub-critical nature of the pure Tayler–Spruit model, we will now reinstate the effect of the more traditional part of $\alpha$ which we parametrize, for the sake of convenience, as

$$\alpha^c(\theta, t) = \alpha_0^c \big(1 + \xi(t)\big) \sin(2\theta) \frac{1}{(1 + q_\alpha^c B^2(\theta, t))}, \tag{8}$$

where $\alpha_0^c$ is a constant and $\xi(t)$ denotes a noise term to be specified further below. The factor $\sin(2\theta)$ ensures the typical north–south asymmetry as it is often assumed for conventional $\alpha - \Omega$ dynamos. Interestingly, the same symmetry argument would also apply to a TI-related, non-oscillatory $\alpha$ term under the influence of an additional poloidal field (Rüdiger, Kitchatinov, and Hollerbach, 2013; Rüdiger *et al.*, 2015a). Therefore, any such non-oscillatory contribution of the TI-related $\alpha$ effect could be consistently absorbed into Equation 8.

### 4.1. Noise-Free Case

Let us start with the noise-free case, *i.e.*, $\xi(t) = 0$, for which we consider first a purely conventional $\alpha - \Omega$ dynamo, by skipping the periodic part completely, *i.e.*, by choosing $\alpha_0^p = 0$. Figure 9 shows the time evolution for increasing intensity of the constant part, *i.e.*, $\alpha_0^c = 0.6$ (a), 0.8 (b), 1 (c), 4 (d), 10 (e) and 40 (f). The other parameters are $\omega_0 = 10\,000$, $q_\alpha^c = 0.8$, $\kappa = 0.5$. While the field clearly dies out for $\alpha_0^c = 0.6$ (a), for $\alpha_0^c = 0.8$ it seems to recover very slowly, and for $\alpha_0^c = 1$, we get a clear dynamo with an oscillatory quadrupole which also prevails for $\alpha_0^c = 4$ (d) and $\alpha_0^c = 10$ (e). At $\alpha_0^c = 40$ (e), the dynamo field undergoes several changes and ends up in a dipole field pulsating with a period of approximately 27 years. Note that we have here extended the time period to 500 years in order to show all relevant transitions which are partly very slow.

What happens now if we complement this standard $\alpha - \Omega$ dynamo with the periodic $\alpha$ term? For the four specific choices $\alpha_0^c = 1, 4, 10, 40$ (*cf.* Figure 9(c) – (f)), we show in Figure 10 the resulting dynamo period when cranking up the value of $\alpha_0^p$. For each considered value of $\alpha_0^c$, we ultimately obtain a clear synchronization to a 22.14-years period when the
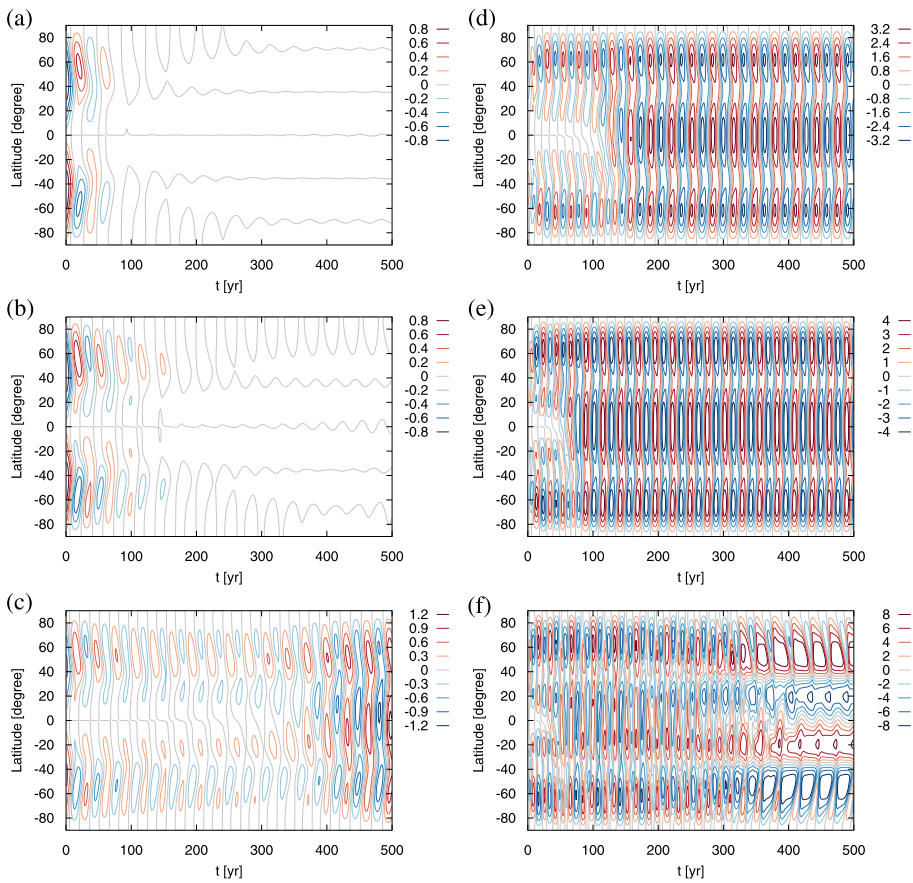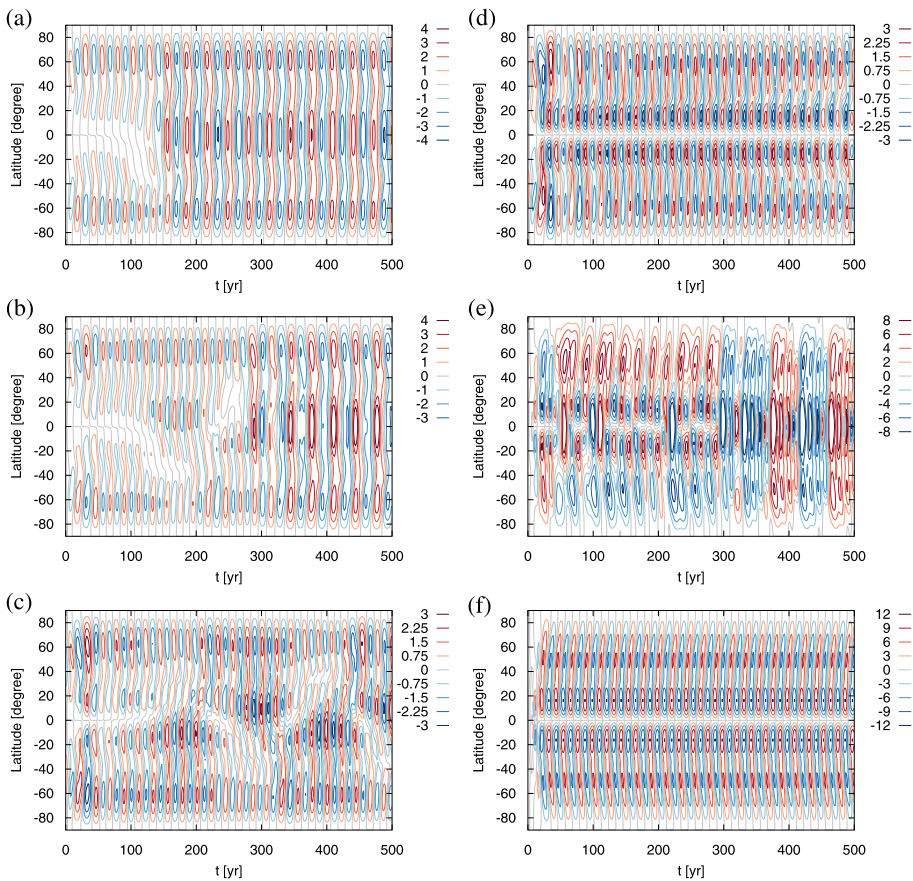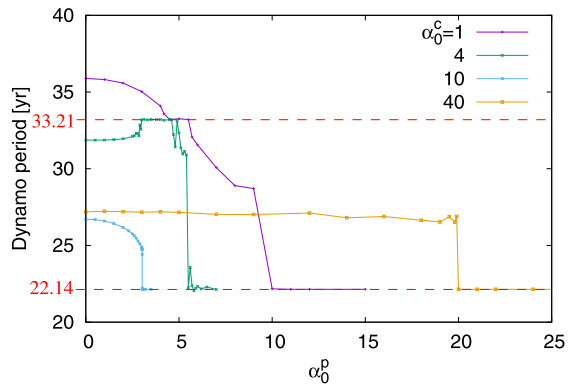
**Figure 9** Behavior of $B(\theta, t)$ of the traditional $\alpha$–$\Omega$ dynamo without periodic term, *i.e.*, with $\alpha_0^p = 0$. The fixed parameters are $\omega_0 = 10\,000$, $\kappa = 0.5$, $q_\alpha^c = 0.8$, $q_\alpha^p = 0.2$, the initial conditions are $s = 1$ and $u = 0.001$, and the varying parameter is $\alpha_0^c = 0.6$ (**a**), 0.8 (**b**), 1 (**c**), 4 (**d**), 10 (**e**), 40 (**f**).

value of $\alpha_0^p$ reaches a certain critical value. In cases that the original period is higher ($\alpha_0^c = 1$ and 4), we also observe an intermediate 2:3 synchronization to a 33.21-years period. Remarkably, the value of $\alpha_0^p$, where the final synchronization to 22.14 years is accomplished, can be significantly smaller than the typical $\alpha_0^p$ needed for the pure Tayler–Spruit dynamo to start (*cf.* Figure 8).

For the specific value $\alpha_0^c = 4$ (*cf.* the green line in Figure 10), Figure 11 illustrates the complexities of this synchronization. While for the low value $\alpha_0^p = 1$ (a) we obtain the nearly unperturbed oscillatory quadrupole, $\alpha_0^p = 4$ (b) yields now the intermediate 2:3 synchronization into a fluctuating quadrupole. Shortly after leaving this 2:3 synchronization regime, $\alpha_0^p = 6$ (c) provides a sort of hemispherical field with 22.14-years period, whose dominating hemisphere is, however, changing with an approximately 200-years periodicity. Increasing $\alpha_0^p$ further to 10 (d), we observe a dipole oscillating with a strong Gnevyshev–Ohl tendency. $\alpha_0^p = 50$ produces a wild transition between oscillatory dipoles and pulsating quadrupoles at later times. Very regular dipole oscillations appear then at $\alpha_0^p = 150$. This way, we obtain a transition from the conventional $\alpha$–$\Omega$ dynamo via a hybrid dynamo to a

**Figure 10** Resonance with the external frequency when increasing $\alpha_0^p$, for four different values of $\alpha_0^c = 1, 4, 10, 40$, whose $\alpha_0^p = 0$ limit corresponds to panels (c), (d), (e) and (f) of Figure 9, respectively.





**Figure 11** Behavior of $B(\theta, t)$ of the traditional $\alpha$–$\Omega$ combined with increasing $\alpha_0^p$. The fixed parameters are $\omega_0 = 10\,000$, $\kappa = 0.5$, $q_\alpha^c = 0.8$, $q_\alpha^p = 0.2$, $\alpha_0^c = 4$, the initial conditions are $s = 1$ and $u = 0.001$, and the varying parameter is $\alpha_0^p = 1$ (**a**), 4 (**b**), 6 (**c**), 10 (**d**), 50 (**e**), 150 (**f**).

**Figure 12** Behavior of $B(\theta, t)$ (**a**), $A(\theta, t)$ (**b**), and $\alpha(\theta, t)$ (**c**). Parameters as in Figure 11, but with $\alpha_0^p = 12$.
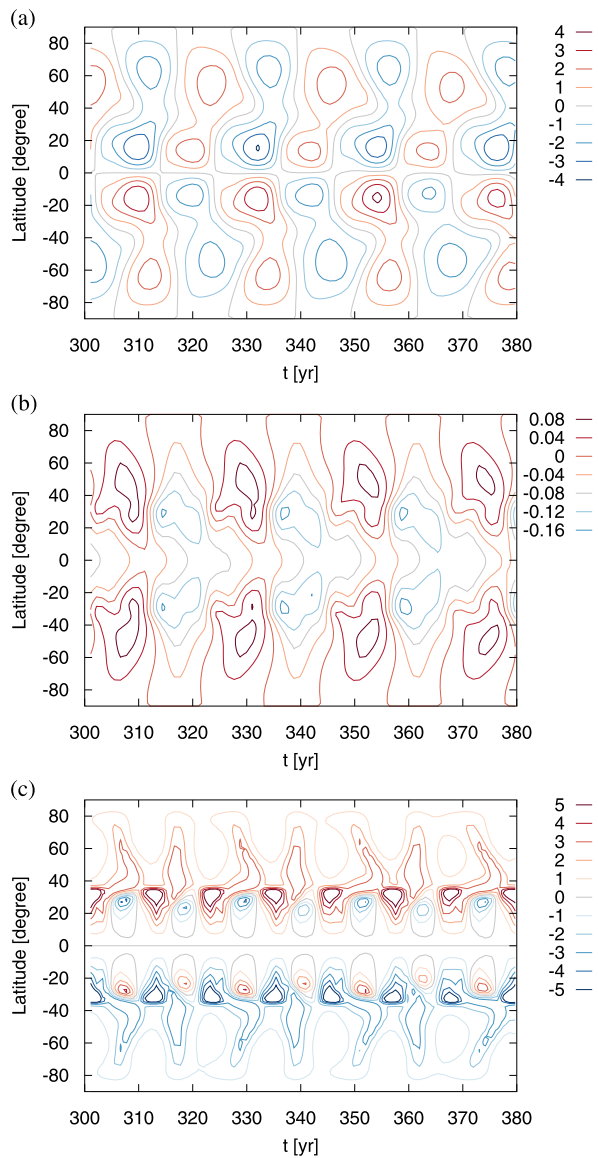


(nearly) pure Tayler–Spruit dynamo, and synchronization starts at a certain fraction of the oscillatory part of $\alpha$.

   More details of this hybrid dynamo behavior can be seen in Figure 12, documenting the special case $\alpha_0^c = 4$ and $\alpha_0^p = 12$ (similar to Figure 11d). Here the direction of the butterfly diagram for low latitudes is not very well expressed. Quite interesting is the $\alpha$ effect of panel (c) which shows now, not surprisingly due to the presence of $\alpha^c$, a preponderance of positive values in the northern, and negative values in the southern hemisphere. The remaining oscillatory part, which has a reasonable amplitude of approximately $0.5 \text{ m s}^{-1}$ (recall the necessary division by 7 to get the physical values), is sufficient to synchronize the entire dynamo.
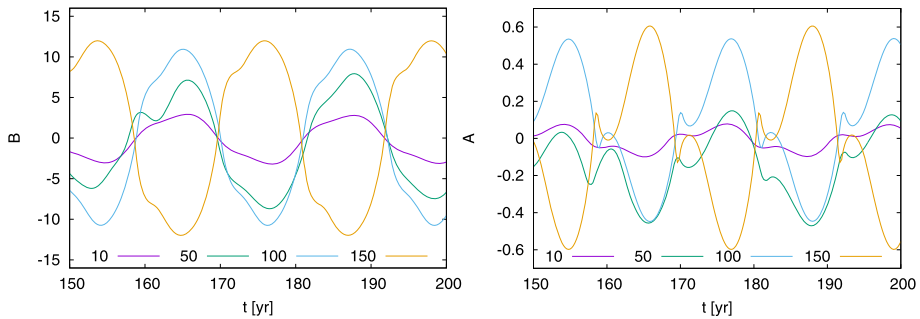
**Figure 13** Detail of Figure 12 for $B(\theta = 72°, t)$ (*left*) and $A(\theta = 72°, t)$ (*right*) for various values of $\alpha_0^p$.

Another interesting aspect becomes visible in Figure 12(a), (b), and is quantified in detail in Figure 13 which shows $B(\theta = 72°, t)$ and $A(\theta = 72°, t)$. It refers to the occurrence of a double peak of the field amplitude, which is even clearer expressed in the poloidal field $A$ than in the toroidal field $B$. This double peak is a quite typical feature of the solar dynamo and has been discussed, *e.g.*, in Karak, Mandal, and Banarjee (2018). It might also be worthwhile to check the relation of this double peak to the so-called "mid-term" periodicities (between 0.5 and 4 years) of the solar activity, as found and discussed by several authors (Obridko and Shelting, 2007; Valdés-Galicia and Velasco, 2008; McIntosh, 2015; Bazylevskaya *et al.*, 2016).

### 4.2. The Role of Noise

Having seen that a conventional $\alpha$–$\Omega$ dynamo with an intrinsic frequency can be synchronized by adding a periodic $\alpha$ term, we ask now about the specific influence of noise on the behavior of these two types of models. In either case, we augment the non-periodic part of $\alpha$ by a noise term $\xi(t)$ defined by the correlator $\langle \xi(t)\xi(t + t_1) \rangle = D^2(1 - |t_1|/t_{\text{corr}})\Theta(1 - |t_1|/t_{\text{corr}})$, which is numerically realized by random numbers with variance $D^2$ which are held constant over a correlation time $t_{\text{corr}}$. In the following, we will choose, somewhat arbitrarily, $t_{\text{corr}} = 0.55$ years, which is at any rate significantly shorter than the solar cycle. We start with a pure $\alpha$–$\Omega$ model with $\alpha_0^p = 0$, $\alpha_0^c = 10$, $\omega_0 = 10\,000$, $q_\alpha^c = 0.8$, $q_\alpha^p = 0.2$, $\kappa = 0.5$, which corresponds to the leftmost point of the blue curve in Figure 10. For $D = 0.3$, the rightmost curves (marked by circles) of Figure 14(a) illustrate three specific noise realizations, which all exhibit long-term, large-amplitude excursions around their linear trends (note that we have used, for the sake of easy comparison, the same scales as in Figure 1). Dicke's ratio for these three curves is shown, using the same colors, in Figure 14(b). Despite large deviations of the individual curves, we observe a clear resemblance to the $\sim N/15$ dependence as typical for a random walk process.

Things are different, though, for the hybrid dynamo. In addition to the parameters indicated above, we choose now $\alpha_0^p = 5$, which lies well in the synchronized part of the blue curve of Figure 10. The resulting three leftmost time series (marked by squares) in Figure 14(a) now remain much closer to the linear trend, without undergoing long-term excursions. It is evident, however, that the noise alleviates any *local* clocking with the periodic forcing, while the *global* clocking is well maintained. Unsurprisingly, Dicke's ratio for these time series in Figure 14(b) is quite close to the ideal curve for a clocked process. This clear difference between a random walk process and a clocked process, as evidenced in our
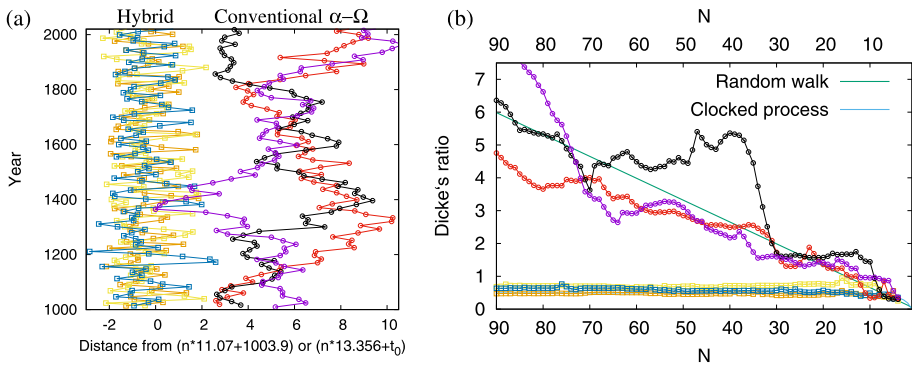
**Figure 14** The role of noise for the conventional $\alpha$–$\Omega$ and the hybrid dynamo model. (**a**) Deviations of the time series from linear functions of the cycle number for three noise realizations in either case. For the conventional $\alpha$–$\Omega$ the three time series (with *circles, on the right side*) undergo long-term excursions, while the time series for the hybrid dynamo (with *squares, on the left side*) remain much closer to the linear trend. (**b**) Dicke's ratio in dependence on the number $N$ of cycles taken into account, for a random walk process (*green line*, converging towards $N/15$), a clocked process (*blue line*, converging towards 0.5), and the two triples of time series as shown in (**a**).

two numerical models, makes it indeed worthwhile to validate or improve Schove's data on which the curves in Figures 1 and 2 were based.

## 5. Modeling Grand Minima

In contrast to the idea of a *hard synchronization* of the basic Hale cycle with planetary tidal forces, as pursued in this paper, much more interest is commonly devoted to the possibility of a *soft modulation* of the solar activity, with particular focus on the Gleissberg, Suess–de Vries, Hallstadt, and Eddy cycles (Jose, 1965; Charvatova, 1997; Abreu *et al.*, 2012; Wolff and Patrone, 2010; Scafetta, 2010, 2014; McCracken, Beer, and Steinhilber, 2014; Cionco and Soon, 2015; Scafetta *et al.*, 2016). While far from being settled (see, *e.g.*, Cameron and Schüssler, 2014 for a critical assessment), any such planetary influence could have enormous consequences for the predictability not only of the solar dynamo but, possibly, of the terrestrial climate, too (Hoyt and Schatten, 1997; Gray *et al.*, 2010; Solanki, Krilova, and Haigh, 2013; Scafetta, 2013; Ruzmaikin and Feynman, 2015; Soon *et al.*, 2014). It is, therefore, worthwhile to figure out whether our model can explain modulations of the solar cycle, including extreme cases such as the Maunder and other grand minima.

We had already seen above (Figures 5(d) and 11(e)) that for some parameter choices transitions between dipoles and quadrupoles can even occur spontaneously, which indicates a high sensitivity of the corresponding dynamo with respect to minor parameter variations. Based on this observation, we study here the transition between the two field topologies when allowing the ratio of $\alpha^p$ to $\alpha^c$ to vary with a long period, for which we take here 550 years just for the sake of concreteness (at a comparably 506-years period, Abreu *et al.*, 2012 found a peak both in the solar modulation potential and the annually averaged planetary torque modulus).

Using the fixed parameters $\omega_0 = 10\,000$, $\alpha_0^c = 1$, $\kappa = 1$ $q_\alpha^p = 0.2$, $q_\alpha^c = 0.8$, we consider now $\alpha_0^p$ in Equation 4 as time-dependent and vary its value between 27 and 90 according to $\alpha_0^p(t) = 90(1 - 0.7\sin^2(2\pi t/1100))$. This function has maxima at $t = 0$, 550 and 1100, and
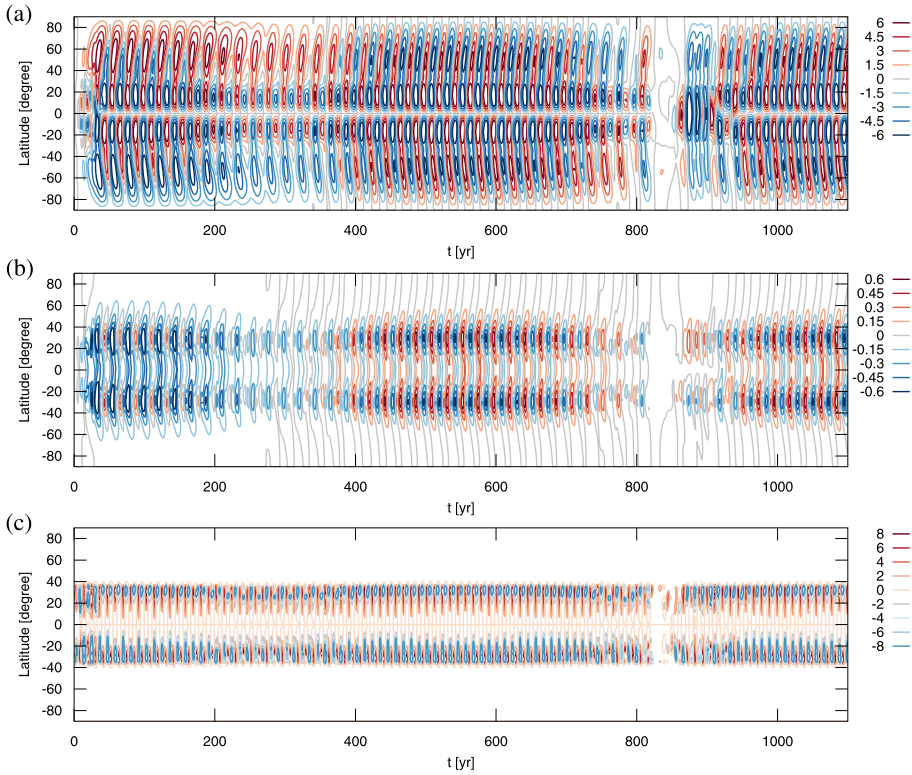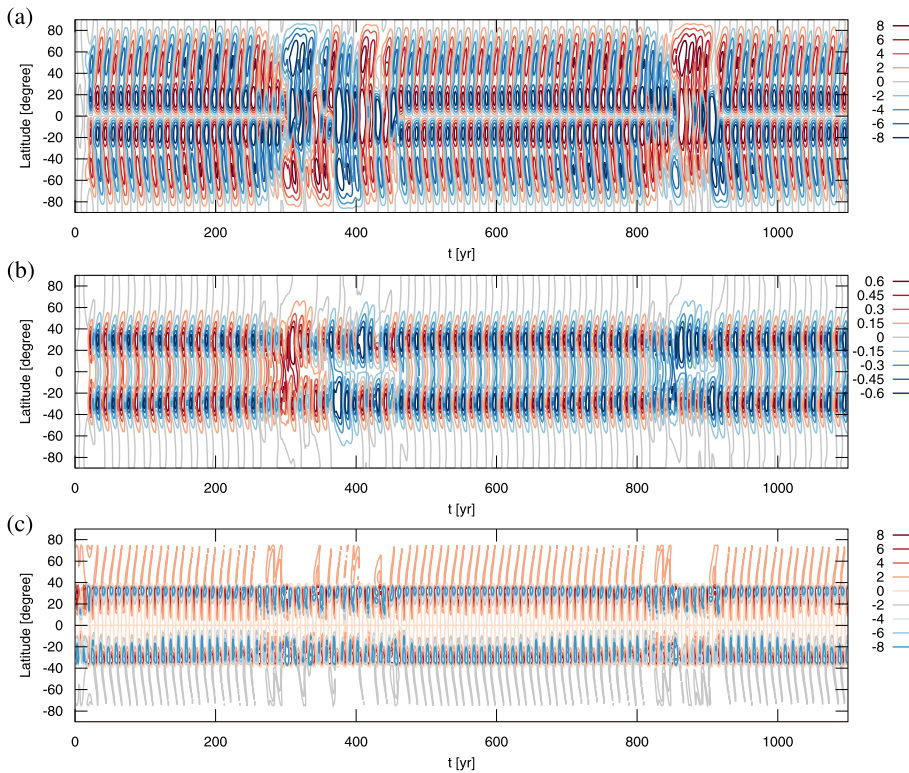
**Figure 15** Behavior of $B(\theta, t)$ (**a**), $A(\theta, t)$ (**b**), and $\alpha(\theta, t)$ (**c**) showing transitions between dipole and quadrupole fields when varying $\alpha_0^p$ according to $\alpha_0^p(t) = 90(1 - 0.7 \sin^2(2\pi t/1100))$. The fixed parameters are $\Omega_0 = 10\,000$, $\alpha_0^c = 1$, $\kappa = 1$ $q_\alpha^p = 0.2$, $q_\alpha^c = 0.8$.

minima at $t = 225$ and 775. Figure 15 shows the results: at the first minimum of $\alpha_0^p$, around $t = 225$, the dipolar field is just weakened and does not undergo a transition to a quadrupole, while exactly this happens at the second minimum, after $t = 775$, where the dipole shortly vanishes and gives way to a quadrupole field before coming back again around $t = 900$. This difference in behavior at the first and second minimum of $\alpha_0^p$ indicates a high sensitivity of these transitions. Note that in particular the transition between quadrupole and dipole looks similar to that after the Maunder minimum (Arlt, 2009; Moss and Sokoloff, 2017).

Most important here is the phase memory during all these transitions. This feature brings us back to the amazing persistence of the solar cycle, even during the Maunder minimum, as it was demonstrated in Figure 1.

Figure 16 shows a similar result which we obtain when varying the loss term $\kappa B^3$ in Equation 1. As noticed above, that term is supposed to account for the field losses due to magnetic buoyancy. Variations of this term might, therefore, be related to variations of the adiabaticity, and hence of the field storage capacity, in the tachocline, an effect that was proposed by Abreu *et al.* (2012) to explain the impact of weak tidal forces on (long-term) variations of the solar dynamo. Again we see that these variations can lead to transitions between dipoles and quadrupoles. This means that, while only a synchronization of $\alpha$ seems to be strong enough to accomplish the "hard synchronization" of the basic Hale cycle, there

**Figure 16** Behavior of $B(\theta, t)$ (**a**), $A(\theta, t)$ (**b**), and $\alpha(\theta, t)$ (**c**) showing transitions between dipole and quadrupole fields when varying $\kappa$ according to $\kappa(t) = 1(1 - 0.6 \sin^2(2\pi t/1100))$. The fixed parameters are $\Omega_0 = 10\,000$, $\alpha_0^c = 4$, $\alpha_0^p(t) = 100$ $q_\alpha^p = 0.2$, $q_\alpha^c = 0.8$.

is still a good chance that the long-term variations of the solar cycle may also result from tidal effects on the adiabaticity in the tachocline.

## 6. Discussion and Outlook

As a sequel to our previous studies (Stefani *et al.*, 2016, 2018), this paper was concerned with the spatio-temporal behavior of a tidally synchronized dynamo of the Tayler–Spruit type, and its combination with a more conventional $\alpha$–$\Omega$-dynamo. Utilizing a solar-like latitudinal dependence of the $\Omega$-effect, and assuming a plausible latitudinal dependence of the TI-related, periodic $\alpha$-effect, we have regularly found dipole or quadrupole fields with 22.14-years periodic oscillations or 11.07-years periodic pulsations. Intermediate states between oscillations and pulsations, reminiscent of the Gnevyshev–Ohl rule, as well as hemispherical fields, were observed, too. Under the influence of noise, the synchronized model maintained its character as a (globally) clocked process, while a conventional $\alpha$–$\Omega$ model had much closer resemblance to a random walk process.

With appropriate changes of the relative weights of the periodic and the non-periodic $\alpha$-terms, or by varying the loss term accounting for magnetic buoyancy, it was easily possible to induce transitions between different field topologies, while maintaining phase co-

herence during all those transitions. The sub-critical nature of the pure Tayler–Spruit type model was confirmed, too.

The considered "hybrid" version of our synchronized dynamo, which builds on the conventional $\alpha$–$\Omega$ concept and requires only weak periodic $\alpha$ forcing for synchronization, is quite attractive for the following reason: In the context of analyzing the two branches of main-sequence stars, separated by the Vaughan–Preston gap (around $2-3$ Gyr, Vaughan and Preston, 1980), the Sun appears as an ordinary, slowly rotating (older) star showing a typical activity period in the usual 10-years range, in contrast to faster rotating younger stars which show partly a shorter and strongly varying ($7.6 \pm 4.9$ years) periodicity, but in general a rather irregular temporal behavior (Soon, Baliunas, and Zhang, 1993; Oláh *et al.*, 2016). A bold explanation for the relation between cycle period and rotation period, as observed for older stars, would have to assert that all of them were synchronized by a similar mechanism as discussed here. Since this scenario is rather unlikely (all those stars would need planetary systems with a dominant tidal periodicity in the same order of 10 years), we are in no way opposed to traditional dynamo concepts yielding typical activity periods in the order of 10 years. We suggest, however, that in particular cases such as our Sun, those conventional dynamos could be synchronized by planetary tidal forcing. Our hybrid version thus remedies the general fitting of our Sun into the cycle period/rotation period relation of older stars with the specific synchronization of the Sun's dynamo as suggested by the time series of Figure 1 and the remarkable behavior of Dicke's ratio shown in Figure 2. Unfortunately, similar statistical arguments as for the Sun, which are based on tens or even hundreds of cycles, cannot be inferred from the much shorter databases as available for other stars (Soon, Baliunas, and Zhang, 1993; Oláh *et al.*, 2016).

Two interesting features, which were already salient in the zero-dimensional model of Stefani *et al.* (2016), have been confirmed in the 1D model: these are the appearance of a double peak of the field (best seen in the poloidal field), and the intermediate emergence of reversed helicities in the two hemispheres. Both effects can indeed be related to corresponding observational facts.
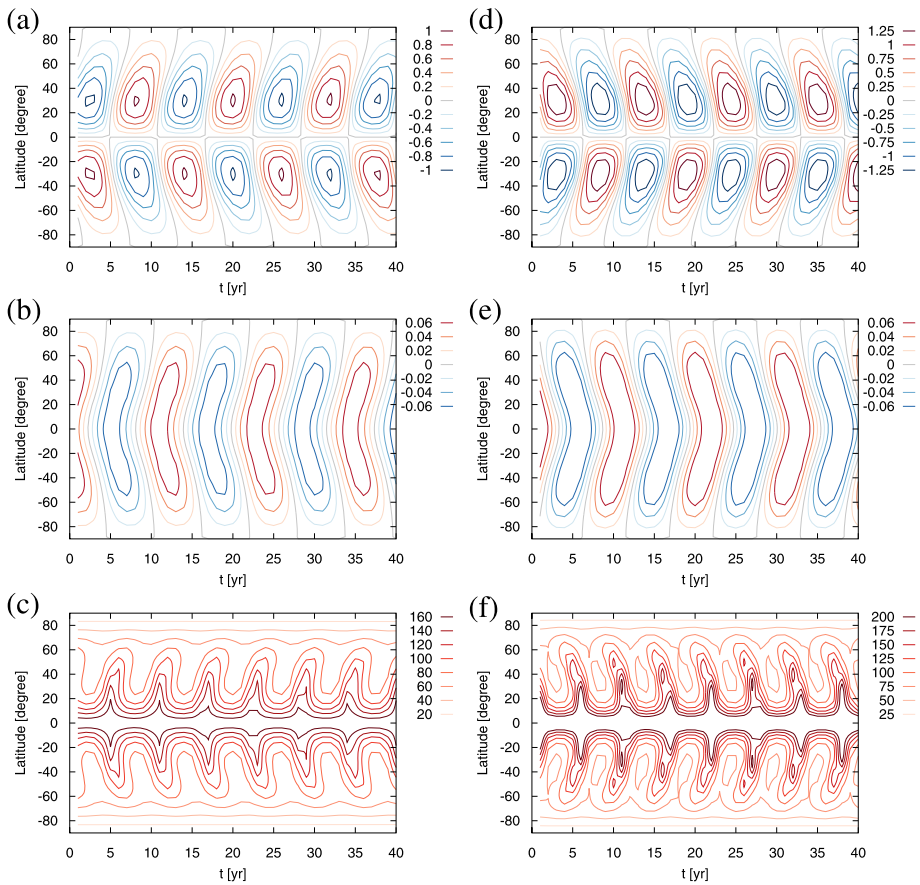
Hence, our Tayler–Spruit type dynamo model, based on a tidally synchronized TI-related $\alpha$-effect, might have acquired greater plausibility by evincing a number of spatio-temporal features which are typical for the solar magnetic field. We hope that these results are promising enough to motivate more advanced 2D or 3D simulations. It remains to be seen whether the evident weaknesses of the model, in particular the unconvincing shape of butterfly diagram, can be mitigated by such an advanced modeling. Just as more traditional concepts of the solar dynamo, our model might still require an enhancement by meridional circulation in order to show butterfly diagrams in their full beauty. It is here where also the specific role of the $\pm 55°$ latitude region for starting the dynamo cycle (McIntosh, 2015) might find an explanation, which could not be provided by our simple 1D model.

We would also point out that the main idea of our model – that the helicity of an $m = 1$ instability can be synchronized even by a weak periodic $m = 2$ tidal perturbation, with the energy content of the instability being essentially unchanged – is not necessarily restricted to the very Tayler instability but might well be applicable to other $m = 1$ instabilities or flow features, too. A preliminary study has shown, for example, a comparable synchronization effect for the $m = 1$ dominated large scale circulation (LSC) in Rayleigh–Bénard convection (Galindo, 2018). Similar synchronization mechanisms have been discussed in connection with the $m = 1$ eigenmode in the von Kármán-sodium (VKS) dynamo experiment (Giesecke, Stefani, and Burguete, 2012; Giesecke, Stefani, and Herault, 2017). It seems also worthwhile to examine the same $\alpha$ synchronization concept for the recently discussed Rossby waves of the tachocline (McIntosh *et al.*, 2017; Dikpati *et al.*, 2017; Zaqarashvili,

2018). The strong dependence of these waves on the gravity parameter would bring back into play the concept of a tidal influence on the adiabaticity as proposed by Abreu *et al.* (2012).

Finally, we note that a completely new perspective for synchronization may arise from the recent observation that positive shear flows, such as in the near-equator parts of the tachocline, are susceptible to a new kind of axisymmetric, double-diffusive MRI, as long as both azimuthal and axial fields are present (Mamatsashvili *et al.*, 2018).

**Figure 17**  Spatio-temporal behavior of a simple $\alpha$–$\Omega$ model with pure $\Omega$-quenching, for two different intensities of the differential rotation, $\omega_0 = 170$ (**a**)–(**c**), and $\omega_0 = 250$ (**d**)–(**f**). The upper two panels (**a**), (**d**) show $B(\theta, t)$, the central two panels (**b**), (**e**) show $A(\theta, t)$, the lower two panels (**c**), (**f**) show $\omega(\theta, t)$. Note the "wrong" butterfly direction for $\omega_0 = 170$ (**a**), and the correct direction for $\omega_0 = 250$ (**d**). In either case, the toroidal flux (**a**), (**d**) is mainly transported along the isolines of $\omega(\theta, t)$ (see (**c**), (**f**)), according to Yoshimura's rule.

# Appendix

In this appendix, we validate our numerical model by considering again the model of Jennings and Weiss (1991) which includes a (not very physical) quenching of the $\Omega$-effect by the back-reaction of the magnetic field in the specific form

$$\omega(\theta, t) = \omega_0 \sin(\theta)/\big(1 + q_\omega B^2(\theta, t)\big), \tag{9}$$

while leaving the $\alpha$-effect unaffected. Fixing $\alpha_0 = -1$ and the quenching parameter $q_\omega = 1$, Figure 17 shows the arising spatio-temporal dynamo behavior for two different values $\omega_0 = 170$ (a), (b), (c) and $\omega_0 = 250$ (d), (e), (f). The first row (a), (d) shows $B(\theta, t)$, the second row shows $A(\theta, t)$, and the third row shows $\omega(\theta, t)$ (we skip $\alpha(\theta) = \alpha_0 \cos(\theta)$ because it is time-independent). Interestingly, depending on the value of $\omega_0$, the system develops a butterfly diagram pointing either away from (a) or towards (d) the equator. In either case, the direction follows basically the isolines of $\omega$; see (c) and (f), according to a theorem by Yoshimura (1975).

# References

Abreu, J.A., Beer, J., Ferriz-Mas, A., McCracken, K.G., Steinhilber, F.: 2012, Is there a planetary influence on solar activity? *Astron. Astrophys.* **548**, A88. DOI.

Arlt, R.: 2009, The butterfly diagram in the eighteenth century. *Solar Phys.* **255**, 143. DOI.

Bazylevskaya, G.A., Kalinin, M.S., Krainev, M.B., Makhmutov, V.S., Svirzhevskaya, A.K., Svirzhevsky, N.S., Stozhkov, Y.I.: 2016, On the relationship between quasi-biennial variations of solar activity, the heliospheric magnetic field and cosmic rays. *Cosm. Res.* **54**, 171. DOI.

Beer, J., Tobias, S., Weiss, N.: 1998, An active Sun throughout the Maunder minimum. *Solar Phys.* **181**, 237. DOI.

Bollinger, C.J.: 1952, A 44.77 year Jupiter–Venus–Earth configuration Sun-tide period in solar-climatic cycles. *Proc. Okla. Acad. Sci.* **33**, 307.

Bonanno, A., Guarnieri, F.: 2017, On the possibility of helicity oscillations in the saturation of the Tayler instability. *Astron. Nachr.* **338**, 516. DOI.

Bonanno, A., Brandenburg, A., Del Sordo, F., Mitra, D.: 2012, Breakdown of chiral symmetry during saturation of the Tayler instability. *Phys. Rev. E* **86**, 016313. DOI.

Callebaut, D.K., de Jager, C., Duhau, S.: 2012, The influence of planetary attractions on the solar tachocline. *J. Atmos. Solar-Terr. Phys.* **80**, 73. DOI.

Cameron, R.H., Schüssler, M.: 2014, No evidence for planetary influence on solar activity. *Astron. Astrophys.* **557**, A83. DOI.

Charbonneau, P.: 2010, Dynamo models of the solar cycle. *Living Rev. Solar Phys.* **7**, 3. DOI.

Charbonneau, P., Christensen-Dalsgaard, J., Henning, R., Larsen, R.M., Schou, J., Thompson, M.J., Tomczyk, S.: 1999, Helioseismic constraints on the structure of the solar tachocline. *Astrophys. J.* **527**, 445. DOI.

Charvatova, I.: 1997, Solar-terrestrial and climatic phenomena in relation to solar inertial motion. *Surv. Geophys.* **18**, 131. DOI.

Chatterjee, P., Mitra, D., Brandenburg, A., Rheinhardt, M.: 2011, Spontaneous chiral symmetry breaking by hydromagnetic buoyancy. *Phys. Rev. E* **84**, 025403. DOI.

Cionco, R.G., Soon, W.: 2015, A phenomenological study of the timing of solar activity minima of the last millennium through a physical modeling of the Sun-planets interaction. *New Astron.* **34**, 164. DOI.

Condon, J.J., Schmidt, R.R.: 1975, Planetary tides and the sunspot cycles. *Solar Phys.* **42**, 529. DOI.

De Jager, C., Versteegh, G.: 2005, Do planetary motions drive solar variability? *Solar Phys.* **229**, 175. DOI.

Dicke, R.H.: 1978, Is there a chronometer hidden deep in the Sun? *Nature* **276**, 676.

Dikpati, M., Cally, P.S., McIntosh, S.W., Heifetz, E.: 2017, The origin of the "Seasons" in space weather. *Sci. Rep.* **7**, 14750. DOI.

Eckhardt, B., Faisst, H., Schmiegel, A., Schneider, T.M.: 2008, Dynamical systems and the transition to turbulence in linearly stable shear flows. *Phil. Trans. Roy. Soc. A* **366**, 1297. DOI.

Ferriz Mas, A., Schmitt, D., Schüssler, M.: 1994, A dynamo effect due to instability of magnetic flux tubes. *Astron. Astrophys.* **289**, 949.

Galindo, V.: 2018, personal communication.

Gellert, M., Rüdiger, G., Hollerbach, R.: 2011, Helicity and alpha-effect by current-driven instabilities of helical magnetic fields. *Mon. Not. Roy. Astron. Soc.* **414**, 2696. DOI.

Giesecke, A., Stefani, F., Burguete, J.: 2012, Impact of time-dependent nonaxisymmetric velocity perturbations on dynamo action of von Kármán-like flows. *Phys. Rev. E* **86**, 066303. DOI.

Giesecke, A., Stefani, F., Herault, J.: 2017, Parametric instability in periodically perturbed dynamos. *Phys. Rev. Fluids* **2**, 053701.

Gnevyshev, M.N., Ohl, A.I.: 1948, On the 22-year cycle of solar activity. *Astron. J.* **25**, 18. DOI.

Gough, D.O.: 1990, On possible origins of relatively short-term variations in the solar structure. *Phil. Trans. Roy. Soc. London A* **330**, 627. DOI.

Grandpierre, A.: 1996, On the origin of solar cycle periodicity. *Astrophys. Space Sci.* **243**, 393. DOI.

Gray, L.J., Beer, J., Geller, M., Haigh, J.D., Lockwood, M., Matthes, K., Cubasch, U., Fleitmann, D., Harrison, G., Hood, L., Luterbacher, J., Meehl, G.A., Shindell, D., van Geel, B., White, W.: 2010, Solar influences on climate. *Rev. Geophys.* **48**, RG4001. DOI.

Hathaway, D.H.: 2010, The solar cycle. *Living Rev. Solar Phys.* **7**, 1. DOI.

Hoyng, P.: 1996, Is the solar cycle timed by a clock? *Solar Phys.* **169**, 253.

Hoyt, D.V., Schatten, K.H.: 1997, *The Role of the Sun in Climate Change*, Oxford University Press, New York.

Hung, C.-C.: 2007, Apparent relations between solar activity and solar tides caused by the planets, NASA/TM-2007-214817.

Jennings, R.L., Weiss, N.O.: 1991, Symmetry breaking in stellar dynamos. *Mon. Not. Roy. Astron. Soc.* **252**, 249. DOI.

Jones, C.A.: 1983, Model equations for the solar dynamo. In: Soward, A.M. (ed.) *Stellar and Planetary Magnetism*, Gordon and Breach, New York, 193.

Jose, P.D.: 1965, Sun's motion and sunspots. *Astron. J.* **70**, 193. DOI.

Jouve, L., Gastine, T., Lignieres, F.: 2015, Three-dimensional evolution of magnetic fields in a differentially rotating stellar radiative zone. *Astron. Astrophys.* **575**, 21. DOI.

Kagan, D., Wheeler, J.C.: 2014, The role of the magnetorotational instability in the Sun. *Astrophys. J.* **787**, A106. DOI.

Karak, B.B., Mandal, S., Banerjee, D.: 2018, Double-peaks of the solar cycle: an explanation from a dynamo model. *Astrophys. J.* **866**, 17. DOI.

Kuzanyan, K.M., Sokoloff, D.: 1997, Half-width of a solar dynamo wave in Parker's migratory dynamo. *Solar Phys.* **173**, 1. DOI.

Mamatsashvili, G., Stefani, F., Hollerbach, R., Rüdiger, G.: 2018, New type of axisymmetric helical magnetorotational instability in rotating flows with positive shear. *Phys. Rev. Lett.*, submitted. arXiv.

McCracken, K.G., Beer, J., Steinhilber, F.: 2014, Evidence for planetary forcing of the cosmic ray intensity and solar activity throughout the past 9400 years. *Solar Phys.* **289**, 3207. DOI.

McIntosh, S.W.: 2015, The solar magnetic activity band interaction and instabilities that shape quasi-periodic variability. *Nat. Commun.* **6**, 6491. DOI.

McIntosh, S.W., Cramer, W.J., Pichardo Marcano, M., Leamon, R.J.: 2017, The detection of Rossby-like waves on the Sun. *Nature Astron.* **11**, 0086. DOI.

Miyahara, H., Masuda, K., Muraki, Y., Kitagawa, H., Nakamura, T.: 2006, Variation of solar cyclicity during the Spoerer minimum. *J. Geophys. Res.* **111**, A03103. DOI.

Moss, D.L., Sokoloff, D.: 2017, Parity fluctuations in stellar dynamos. *Astron. Rep.* **61**, 878. DOI.

Obridko, V.N., Shelting, B.D.: 2007, Occurrence of the 1.3-year periodicity in the large-scale solar magnetic field for 8 solar cycles. *Adv. Space Res.* **40**, 1006. DOI.

Okhlopkov, V.P.: 2014, The 11-year cycle of solar activity and configurations of the planets. *Moscow Univ. Phys. Bull.* **69**, 257. DOI.

Okhlopkov, V.P.: 2016, The gravitational influence of Venus, the Earth, and Jupiter on the 11-year cycle of solar activity. *Moscow Univ. Phys. Bull.* **71**, 440. DOI.

Oláh, K., Kővári, Zs., Petrovay, K., Soon, W., Baliunas, S., Kolláth, Z., Vida, K.: 2016, Magnetic cycles at different ages of stars. *Astron. Astrophys.* **590**, A133. DOI.

Öpik, E.: 1972, Solar-planetary tides and sunspots. I. *Astron. J.* **10**, 298.

Palus, M., Kurths, J., Schwarz, U., Novotna, D., Charvatova, I.: 2000, Is the solar activity cycle synchronized with the solar inertial motion? *Int. J. Bifurc. Chaos* **10**, 2519. DOI.

Parker, E.N.: 1955, Hydromagnetic dynamo models. *Astrophys. J.* **122**, 293. DOI.

Pipin, V.V., Zhang, H., Sokoloff, D.D., Kuzanyan, K.M., Gao, Y.: 2013, The origin of the helicity hemispheric sign rule reversals in the mean-field solar-type dynamo. *Mon. Not. Roy. Astron. Soc.* **435**, 2581. DOI.

Pitts, E., Tayler, R.J.: 1985, The adiabatic stability of stars containing magnetic-fields. 6. The influence of rotation. *Mon. Not. Roy. Astron. Soc.* **216**, 139. DOI.

Poluianov, S., Usoskin, I.: 2014, Critical analysis of a hypothesis of the planetary tidal influence on solar activity. *Solar Phys.* **289**, 2333. DOI.

Proctor, M.R.E.: 2007, Effects of fluctuations on $\alpha\Omega$ dynamo models. *Mon. Not. Roy. Astron. Soc.* **382**, L39. DOI.

Roald, C.B., Thomas, J.H.: 1997, Simple solar dynamo models with variable $\alpha$ and $\omega$ effects. *Mon. Not. Roy. Astron. Soc.* **288**, 551. DOI.

Rüdiger, G., Kitchatinov, L.L., Hollerbach, R.: 2013, *Magnetic Processes in Astrophysics*, Wiley, Berlin.

Rüdiger, G., Gellert, M., Hollerbach, R., Schultz, M., Stefani, F.: 2015a, Stability and instability of hydromagnetic Taylor-Couette flows. *Phys. Rep.* **741**, 1. DOI.

Rüdiger, G., Schultz, M., Gellert, M., Stefani, F.: 2015b, Subcritical excitation of the current-driven Tayler instability by super-rotation. *Phys. Fluids* **28**, 014105. DOI.

Ruzmaikin, A., Feynman, J.: 2015, The Earth's climate at minima of centennial Gleissberg cycles. *Adv. Space Res.* **56**, 1590. DOI.

Scafetta, N.: 2010, Empirical evidence for a celestial origin of the climate oscillations and its implications. *J. Atmos. Solar-Terr. Phys.* **72**, 951. DOI.

Scafetta, N.: 2013, Discussion on climate oscillations: CMIP5 general circulation models versus a semi-empirical harmonic model based on astronomical cycles. *Earth-Sci. Rev.* **126**, 321. DOI.

Scafetta, N.: 2014, The complex planetary synchronization structure of the solar system. *Pattern Recogn. Phys.* **2**, 1. DOI.

Scafetta, N., Milani, F., Bianchini, A., Ortolani, S.: 2016, On the astronomical origin of the Hallstatt oscillation found in radiocarbon and climate records throughout the Holocene. *Earth-Sci. Rev.* **162**, 24. DOI.

Schmalz, S., Stix, M.: 1991, An alpha–Omega dynamo with order and chaos. *Astron. Astrophys.* **245**, 654.

Schove, D.J.: 1955, The sunspot cycle, 649 B.C. to A.D. 2000. *J. Geophys. Res.* **60**, 127.

Schove, D.J.: 1983, *Sunspot Cycles*, Hutchinson Ross Publishing Company, Stroudsburg.

Seilmayer, M., Stefani, F., Gundrum, T., Weier, T., Gerbeth, G., Gellert, M., Rüdiger, G.: 2012, Experimental evidence for Tayler instability in a liquid metal column. *Phys. Rev. Lett.* **108**, 244501. DOI.

Sokoloff, D., Nesme-Ribes, E.: 1994, The Maunder minimum: A mixed-parity dynamo mode? *Astron. Astrophys.* **288**, 293.

Solanki, S.K., Krilova, N.A., Haigh, J.D.: 2013, Solar irradiance variability and climate. *Annu. Rev. Astron. Astrophys.* **51**, 311. DOI.

Soon, W.H., Baliunas, S.L., Zhang, Q.: 1993, An interpretation of cycle periods of stellar chromospheric activity. *Astrophys. J.* **414**, L33. DOI.

Soon, W., Herrera, V.M., Selvaraj, K., Traversi, R., Usoskin, I., Chen, C.A., Lou, J.Y., Kao, S.L., Carter, R.M., Pipin, V., Seven, M., Becagli, S.: 2014, A review of Holocene solar-linked climatic variation on centennial to millennial timescales: Physical processes, interpretative frameworks and a new multiple cross-wavelet transform algorithm. *Earth-Sci. Rev.* **134**, 1. DOI.

Spruit, H.: 2002, Dynamo action by differential rotation in a stably stratified stellar interior. *Astron. Astrophys.* **381**, 923. DOI.

Stefani, F., Kirillov, O.N.: 2015, Destabilization of rotating flows with positive shear by azimuthal magnetic fields. *Phys. Rev. E* **92**, 051001(R). DOI.

Stefani, F., Giesecke, A., Weber, N., Weier, T.: 2016, Synchronized helicity oscillations: A link between planetary tides and the solar cycle? *Solar Phys.* **291**, 2197. DOI.

Stefani, F., Galindo, V., Giesecke, A., Weber, N., Weier, T.: 2017, The Tayler instability at low magnetic Prandtl numbers: chiral symmetry breaking and synchronizable helicity oscillations. *Magnetohydrodynamics* **53**, 169.

Stefani, F., Giesecke, A., Weber, N., Weier, T.: 2018, On the synchronizability of Tayler–Spruit and Babcock–Leighton type dynamos. *Solar Phys.* **293**, 12. DOI.

Takahashi, K.: 1968, On the relation between the solar activity cycle and the solar tidal force induced by the planets. *Solar Phys.* **3**, 598. DOI.

Tayler, R.J.: 1973, The adiabatic stability of stars containing magnetic fields-I: Toroidal fields. *Mon. Not. Roy. Astron. Soc.* **161**, 365. DOI.

Valdés-Galicia, J.F., Velasco, V.M.: 2008, Variations of mid-term periodicities in solar activity physical phenomena. *Adv. Space Res.* **41**, 297. DOI.

Vaughan, A.H., Preston, G.W.: 1980, A survey of chromospheric Ca II H and K emission in field stars of the solar neighborhood. *Publ. Astron. Soc. Pac.* **92**, 385. DOI.

Weber, N., Galindo, V., Stefani, F., Weier, T., Wondrak, T.: 2013, Numerical simulation of the Tayler instability in liquid metals. *New J. Phys.* **15**, 043034. DOI.

Weber, N., Galindo, V., Stefani, F., Weier, T.: 2015, The Tayler instability at low magnetic Prandtl numbers: between chiral symmetry breaking and helicity oscillations. *New J. Phys.* **17**, 113013. DOI.

Weiss, N.O., Tobias, S.M.: 2016, Supermodulation of the Sun's magnetic activity: the effect of symmetry changes. *Mon. Not. Roy. Astron. Soc.* **456**, 2654. DOI.

Wilmot-Smith, A.L., Nandy, D., Hornig, G., Martens, P.C.H.: 2006, A time delay model for solar and stellar dynamos. *Astrophys. J.* **652**, 696. DOI.

Wilson, I.R.G.: 2013, The Venus–Earth–Jupiter spin–orbit coupling model. *Pattern Recogn. Phys.* **1**, 147. DOI.

Wolf, R.: 1859, Extract of a letter to Mr. Carrington. *Mon. Not. Roy. Astron. Soc.* **19**, 85.

Wolff, C.L., Patrone, P.N.: 2010, A new way that planets can affect the Sun. *Solar Phys.* **266**, 227. DOI.

Wood, K.: 1972, Sunspots and planets. *Nature* **240**(5376), 91. DOI.

Wood, T.: 2010, The solar tachocline: A self-consistent model of magnetic confinement. Dissertation, University of Cambridge, Cambridge.

Yoshimura, H.: 1975, Solar-cycle dynamo wave propagation. *Astrophys. J.* **201**, 740. DOI.

Zahn, J.-P., Brun, A.S., Mathis, S.: 2007, On magnetic instabilities and dynamo action in stellar radiation zones. *Astron. Astrophys.* **474**, 145. DOI.

Zaqarashvili, T.: 2018, Equatorial magnetohydrodynamic shallow water waves in the solar tachocline. *Astrophys. J.* **856**, 32. DOI.

Zhang, H.Q., Sakurai, T., Pevtsov, A., Gao, Y., Xu, H.Q., Sokoloff, D., Kuzanyan, K.: 2010, A new dynamo pattern revealed by solar helical magnetic fields. *Mon. Not. Roy. Astron. Soc.* **402**, L30. DOI.